

A global ocean carbon climatology: Results from Global Data Analysis Project (GLODAP)

R. M. Key,¹ A. Kozyr,² C. L. Sabine,³ K. Lee,⁴ R. Wanninkhof,⁵ J. L. Bullister,³
R. A. Feely,³ F. J. Millero,⁶ C. Mordy,³ and T.-H. Peng⁵

Received 25 February 2004; revised 13 September 2004; accepted 1 November 2004; published 29 December 2004.

[1] During the 1990s, ocean sampling expeditions were carried out as part of the World Ocean Circulation Experiment (WOCE), the Joint Global Ocean Flux Study (JGOFS), and the Ocean Atmosphere Carbon Exchange Study (OACES). Subsequently, a group of U.S. scientists synthesized the data into easily usable and readily available products. This collaboration is known as the Global Ocean Data Analysis Project (GLODAP). Results were merged into a common format data set, segregated by ocean. For comparison purposes, each ocean data set includes a small number of high-quality historical cruises. The data were subjected to rigorous quality control procedures to eliminate systematic data measurement biases. The calibrated 1990s data were used to estimate anthropogenic CO₂, potential alkalinity, CFC watermass ages, CFC partial pressure, bomb-produced radiocarbon, and natural radiocarbon. These quantities were merged into the measured data files. The data were used to produce objectively gridded property maps at a 1° resolution on 33 depth surfaces chosen to match existing climatologies for temperature, salinity, oxygen, and nutrients. The mapped fields are interpreted as an annual mean distribution in spite of the inaccuracy in that assumption. Both the calibrated data and the gridded products are available from the Carbon Dioxide Information Analysis Center. Here we describe the important details of the data treatment and the mapping procedure, and present summary quantities and integrals for the various parameters. *INDEX TERMS:* 1635 Global Change: Oceans (4203); 4806 Oceanography: Biological and Chemical: Carbon cycling; 4845 Oceanography: Biological and Chemical: Nutrients and nutrient cycling; 4860 Oceanography: Biological and Chemical: Radioactivity and radioisotopes; *KEYWORDS:* carbon, distribution, inventory

Citation: Key, R. M., A. Kozyr, C. L. Sabine, K. Lee, R. Wanninkhof, J. L. Bullister, R. A. Feely, F. J. Millero, C. Mordy, and T.-H. Peng (2004), A global ocean carbon climatology: Results from Global Data Analysis Project (GLODAP), *Global Biogeochem. Cycles*, 18, GB4031, doi:10.1029/2004GB002247.

1. Introduction

[2] The ocean plays an important role in the carbon cycle on seasonal to millennial timescales. During the 1980s the potential for global climate change initiated by human activity developed from a possibility to a generally accepted belief. This led to a significant increase in the attention given to carbon cycle research. Researchers always recognized that the only way to predict the

influence of anthropogenic “greenhouse” gases on future climate was numerical models. To be of value for prediction, these models had to be able to account for carbon cycling, both carbon distributions within the reservoirs and exchanges between them. Since it is impossible to test the accuracy of a model prediction of future climate change, the only method to judge model performance is comparison to data. That is, if a model cannot reproduce the current state of the environment with reasonable accuracy, then predictions from that model are suspect at least to the level of the data/model difference. By the end of the 1980s the best ocean models appeared to be able to reproduce the known oceanic distribution of parameters pertinent to studies of the ocean carbon cycle. Progress was beginning to be limited by the quantity and quality of the existing measurements. Here we describe the results of a project designed to reverse that situation.

[3] The Geochemical Ocean Sections Program (GEOSECS) carried out during the 1970s provided the first high quality global data set that included the chemical parameters necessary to study the distribution and cycling of carbon in the ocean [Craig, 1972, 1974; Craig and

¹Atmospheric and Oceanic Sciences, Princeton University, Princeton, New Jersey, USA.

²Carbon Dioxide Information Analysis Center, Oak Ridge National Laboratory, Oak Ridge, Tennessee, USA.

³Pacific Marine Environmental Laboratory, NOAA, Seattle, Washington, USA.

⁴School of Environmental Science and Engineering, Pohang University of Science and Technology, Pohang, Republic of Korea.

⁵Atlantic Oceanographic and Meteorological Laboratory, NOAA, Miami, Florida, USA.

⁶Rosenstiel School of Marine and Atmospheric Sciences, University of Miami, Miami, Florida, USA.

Turekian, 1976, 1980]. GEOSECS data provided the foundation on which much of our current understanding of ocean chemistry and biogeochemistry is based. GEOSECS consisted of 316 oceanographic stations which more or less occupied the center of the major ocean basins. Of importance to the ocean carbon cycle were measurements of total dissolved inorganic carbon (henceforth DIC), total alkalinity (henceforth TA), stable carbon isotopes ($\delta^{13}\text{C}$), and the transient tracers tritium (^3H) and radiocarbon ($\Delta^{14}\text{C}$), as well as the more commonly measured temperature, salinity, oxygen, and nutrients (nitrate, phosphate, and silicate). The accuracy of these GEOSECS measurements redefined the standard for “high-quality data” of the period and in most cases are still considered high quality. The exceptions include TA and DIC, which were rather precise but occasionally inaccurate, due to the lack of a standard reference material, and some of the $\delta^{13}\text{C}$ measurements which were contaminated [Kroopnick, 1985].

[4] During the 1990s, three major ocean sampling expeditions were completed: the World Ocean Circulation Experiment (WOCE; in this document, “WOCE” refers only to the hydrographic sampling portion of that program, i.e., WOCE/WHP), the Joint Global Ocean Flux Study (JGOFS), and the Ocean Atmosphere Carbon Exchange Study (OACES). WOCE and JGOFS were international collaborations, while OACES was a NOAA (National Oceanographic and Atmospheric Administration) project. The OACES program and WOCE were survey-type studies, while JGOFS was primarily process oriented. The specific goals of these programs were to better understand ocean circulation, biogeochemistry, and air-sea exchange processes for carbon, to provide a baseline for determining future changes in the ocean, and to develop numerical models that could be used to predict the influence of anthropogenic factors on global climate change. While these three programs were planned, organized, and funded differently, there was significant coordination and collaboration between them. For instance, the carbon sampling and analysis (DIC, TA, pH, and/or pCO_2) on WOCE cruises was a JGOFS project; university scientists participated in OACES cruises; and JGOFS incorporated time series stations at fixed locations (Hawaii and Bermuda), while WOCE had a suite of sections that were repeatedly occupied in addition to the one-time survey sections. With a few intentional exceptions, the programs covered different ocean regions, thus improving the combined global coverage.

[5] Each program incorporated elements designed to provide information that could be applied to global climate change questions. During the field work phase of these three programs the U.S. CO_2 Science Team (composed of the investigators making carbon measurements, supported by D.O.E. and led by John Downing) directed the carbon measurement components of the programs. Once the field work was completed, a subgroup of the Science Team cooperated to produce a merged-calibrated data set and to estimate various parameters pertinent to global climate change. This collaboration continues and is known as the Global Ocean Data Analysis Project (GLODAP). The initial goals of GLODAP were (1) to produce an easily usable,

fully calibrated global data set based on WOCE, JGOFS and OACES measurements, (2) to make uniformly calculated estimates of the oceanic distribution, changes, and inventory of anthropogenic CO_2 , (3) to better describe the aqueous biogeochemistry of inorganic carbon in the ocean, (4) to describe the oceanic distribution and inventory of natural and bomb-produced radiocarbon and to investigate changes in the bomb transient, (5) to produce gridded fields of the various measured and calculated parameters that could be used either as boundary conditions for numerical ocean models or against which model performance could be judged, and (6) to make both the data and the gridded fields publicly available.

[6] Subsets of the data described here have been used to address the second and third goals. That work was done on an ocean by ocean basis as the results became available and the final ocean data sets were compiled. Sabine *et al.* [1999, 2002a] and Lee *et al.* [2003] estimated the anthropogenic CO_2 distribution and inventory for the Indian, Pacific, and Atlantic oceans, respectively. Details in the calculations varied, but all were based on the method devised by Gruber *et al.* [1996] and Gruber [1998]. The global synthesis for anthropogenic CO_2 was given by Sabine *et al.* [2004]. In a similar manner, the inorganic carbon chemistry for the three oceans was described by Sabine *et al.* [2002b], Feely *et al.* [2001, 2002] and Chung *et al.* [2003, 2004]. Feely *et al.* [2004] published a global summary of the carbonate work. Because of the required analytical time, the radiocarbon analysis has lagged significantly; however, the Pacific data have been published [Key, 1996; Key *et al.*, 1996, 2002; Stuiver *et al.*, 1996] in addition to brief scientific summaries [Key, 1997, 2001; Schlosser *et al.*, 2001; Matsumoto and Key, 2004; Matsumoto *et al.*, 2004]. Additionally, Rubin and Key [2002] published an improved method to separate the natural and bomb-produced radiocarbon which was based on the strong linear correlation between potential alkalinity and natural radiocarbon.

[7] Preliminary versions of the gridded GLODAP fields were used in the Ocean Carbon-Cycle Model Intercomparison Project (OCMIP). Orr *et al.* [2001] examined anthropogenic CO_2 uptake during the first phase OCMIP that included four different models. Dutay *et al.* [2002] compared the performance of 13 ocean models in a study of upper ocean ventilation using CFC-11. Additional information about OCMIP is available (<http://www.ipsl.jussieu.fr/OCMIP/>).

[8] Here we address GLODAP goals one and five. First, we describe the data assembly and calibration procedures, and then the objective mapping method. Both the data and the gridded products as well as significant other unpublished information are freely available via the internet (http://cdiac.esd.ornl.gov/oceans/glodap/glodap_home.htm). Users of the GLODAP bottle data sets are strongly cautioned that they are not a simple merge of the data, but a synthetic product. In many cases, adjustments/calibrations have been applied to the data. The adjustments are based on three important assumptions: (1) that the deep ocean hydrography and circulation have been in steady state for the time period covered by the data, (2) that oceanic property distributions, away from the surface and boundaries of all

types, tend to be smooth, and (3) that the experience of the authors (and others) was of value in determining the relative quality of various measurements. The first assumption was not applied to parameters in regions known to be changing due to anthropogenic influences such as DIC, $\delta^{13}\text{C}$, and the transient tracers. The second and third assumptions were important both for the initial quality control check (QC) and for the various adjustments. Both were applied somewhat subjectively and nonuniformly because numerous people were involved. This procedure means that the data set may be subject to erroneous “outlier rejection” problems when unexpected features, for example “Meddies” (mid-depth lenses of anomalously warm, saline Mediterranean water) in the North Atlantic [McDowell and Rossby, 1978] occur in an otherwise relatively uniform background field. That is, some of the data flagged as “questionable” or “bad” during the initial quality control procedure may be real, and/or some of the adjustments applied may have been incorrect. In most cases, the WOCE data were also treated as synoptic in spite of the fact that the collection period covered a decade. In the surface ocean the problems are more severe, since this data set is far too small to adequately address seasonal or interannual changes.

2. Specific Carbon Issues

[9] The inorganic carbon system in the ocean can be described by measuring any two of the four possible parameters: DIC, TA, pH, and pCO_2 . When the WOCE field program began in 1990, certified reference materials (CRM) did not exist, the modern coulometer for DIC [Robinson and Williams, 1991; Goyet and Hacker, 1992] did not exist, and there was no consensus on which of the possible parameter measurements provided the best system description. Also, there was no general agreement on which published estimate of the carbonate equilibrium constants was optimal.

[10] During the field work, three developments radically altered the situation. Dickson and Goyet [Department of Energy, 1994] published a handbook describing ocean carbon chemistry in detail, giving analytical methods for measurement, and showing examples of the important calculations, conversions, etc. A large portion of this information existed in the literature, but was so dispersed (and rife with errors in many cases [see Lewis and Wallace, 1998]) that significant confusion existed. Second, as part of JGOFS, A. Dickson and coworkers at Scripps Institution of Oceanography developed a reliable CRM for shipboard DIC analysis. The CRM was subsequently proven reliable for TA measurements [Millero et al., 1998b; Dickson, 2001; Dickson et al., 2003]. The availability and adoption of a CRM is the greatest contributory factor to the high degree of accuracy in the new carbon measurements. Third was the development and production of the SOMMA (single-operator multiparameter metabolic analyzer) at the University of Rhode Island for the analysis of seawater DIC [Johnson et al., 1993]. This instrument was a vast improvement over previous designs and routinely produced very precise measurements.

[11] Most U.S. investigators restricted carbon measurement to DIC and TA when only two of the four parameters

were measured. On OACES cruises, more than two carbon parameters were always measured. By overdetermining the system, it was possible to investigate the applicability of the carbon equilibrium constants [e.g., Lee et al., 1996; Wanninkhof et al., 1998; McElligott et al., 1998; Millero et al., 2002]. Mojica Prieto and Millero [2002] demonstrated that the Mehrbach constants were more reliable than other studies. For all GLODAP calculations, the Mehrbach et al. [1973] constants as refit by Dickson and Millero [1987] were used. One additional step was taken for the Indian Ocean survey. While the various legs were run by different research groups, all groups shared the same equipment and chemicals. This final step was largely responsible for the exceptionally high quality of the Indian Ocean carbon data.

3. Data Set Construction

[12] The GLODAP data set consists of 9618 hydrographic stations collected on 95 cruises between 1985 and 1999, and 2393 historical hydrographic stations from 21 cruises occupied between 1972 and 1990. Here we use “WOCE stations/cruises/data” to refer to stations occupied as part of either WOCE, JGOFS, or OACES field work and slightly older cruises officially designated as WOCE sections (for example, the Long-Lines cruises P01, P03, and P04 occupied in the late 1980s). “Historical stations/cruises” refers to all other data. No data older than GEOSECS are included due to difficulty in obtaining the data and to the generally lower quality standards that existed. All stations included in the GLODAP data base (version 1.1) are shown in Figure 1.

[13] Data were chosen to provide high-quality global coverage. Most of the data sets were received from the data centers associated with the individual research programs. Additional data were received directly from chief scientists and individual investigators. Significant priority was given to cruises that included the carbon parameters of direct interest to GLODAP goals; however, a limited number of cruises without carbon were included to provide more complete hydrographic, nutrient, and oxygen coverage. cursory investigation indicates that the GLODAP hydrography, nutrients, and oxygen are sufficiently dense to reasonably approximate larger (annual mean) compilations such as provided by Conkright et al. [2002]. Parameters included in the GLODAP bottle data files and metadata for the cruises and investigators are available at the CDIAC website along with the data files. Details of the database construction are in Appendix A. Here only the briefest outline is given.

[14] New data were converted to a common format, and existing quality control (QC) flags were checked. Missing QC flags were assigned using WOCE conventions. Any routinely calculated parameters that existed in the files were discarded. Parameter units were converted to WOCE convention as required [Joyce and Corry, 1994]. Once the decision was made on which cruises were to be included in an ocean compilation, the following steps were executed using a series of semi-automated computer routines:

[15] 1. The data from each cruise were reduced to a defined parameter list and column ordered; then calibration factors and/or adjustments were applied (tables of the

GLODAP Stations

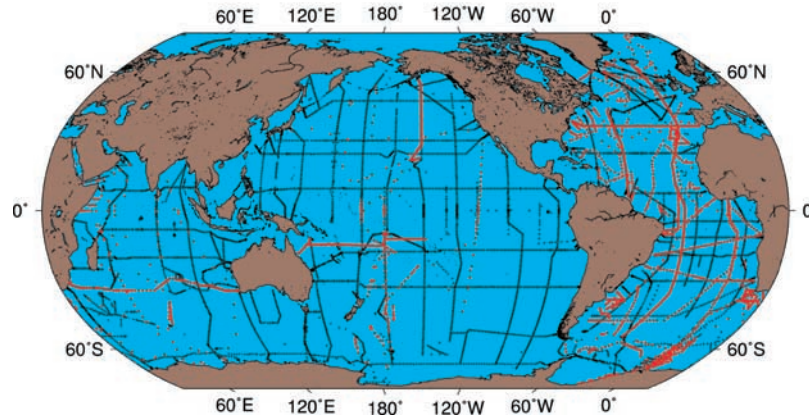


Figure 1. Historical stations are shown in red and are primarily composed of results from the GEOSECS, TTO, SAVE, and INDIGO expeditions. High-quality temperature, salinity, oxygen, and nutrient data exist for almost all stations.

correction factors are available with the data files at the CDIAC web site). The individual cruises for each ocean were merged into a single file, adjusting the original station numbers in a manner that guaranteed uniqueness yet allowed the original number to be easily recovered (equations (A1) and (A2), Appendix A).

[16] 2. Cruise year values were made Y2K compliant. Missing bottom depths were approximated from a global topography. When multiple locations were given for a station, the one indicating position when the CTD cast was at the bottom was chosen. Stations with no reported samples were deleted.

[17] 3. All values flagged “questionable” (“3”) or “bad” (“4”) were deleted from the merged data set. “Replicate” flag values (“6”) were changed to “good” (“2”). “Not reported” flag values (“5”) and “sample collected” (“1”) flag values were changed to “good” in the instances where there actually was a good value and to “missing” (“9”) otherwise. Values flagged “approximated” (“0”) were left as is. The other possible WOCE QC flag values were almost never used (a few CFC values flagged “manual GC integration” (“7”) were changed to “2,” “3,” or “4” during initial screening), so this procedure reduced the possible QC flag values to either approximated, good or not measured (“0,” “2,” or “9”).

[18] 4. Missing Rosette cast values for salinity, nutrients, and oxygen were approximated by constrained vertical interpolation. Any existing nutrient and oxygen values for large volume Gerard samples were discarded and replaced with estimates derived by constrained vertical interpolation using Rosette cast data from the same station.

[19] 5. Potential temperature, potential density (σ_0 , σ_1 , σ_2 , σ_3 , σ_4), and apparent oxygen utilization (AOU) were calculated.

[20] 6. Partial pressure and “age” were calculated for CFC-11 and CFC-12; bomb and natural radiocarbon estimates and radiocarbon age were calculated. All of these were appended to the existing data file.

[21] 7. Subsets of the data were transferred to various GLODAP members responsible for anthropogenic CO_2 estimates. Once finalized, these estimates were merged into the data files.

[22] 8. The entire data file was truncated to single precision and written as a comma separated ASCII file without regard to the number of decimal places retained. This is a shortcoming of the procedure, since insignificant digits exist in all calculated parameters.

[23] 9. The bottle data files were posted to the GLODAP web site (http://cdiac.esd.ornl.gov/oceans/glodap/Glodap_home.htm). CDIAC (A. Kozyr) translated the files into Ocean Data View format [Schlitzer, 2000] (Ocean Data View, 2003, is available at <http://www.awi-bremerhaven.de/GEO/ODV>).

4. Mapping Procedure

[24] The final bottle data files were used to create property maps on 33 depth surfaces. The list of mapped parameters includes total alkalinity ($\mu\text{mol/kg}$), potential alkalinity ($\mu\text{mol/kg}$), total dissolved inorganic carbon ($\mu\text{mol/kg}$), anthropogenic CO_2 ($\mu\text{mol/kg}$), $\Delta^{14}\text{C}$ (‰), bomb-produced ^{14}C (‰), natural (background or pre-bomb) $\Delta^{14}\text{C}$ (‰), CFC-11 (pmol/kg), pCFC-11 (patm), CFC-12 (pmol/kg), and pCFC-12 (patm).

[25] For DIC and CFCs, only WOCE era data were used for surfaces extending from 0 m through 1200 m. For the deeper maps and for all of the TA and potential alkalinity maps, the entire data set was used. No attempt was made to adjust the anthropogenically influenced parameters to a single date. We believe that these adjustments would produce errors approximately equal to those incurred by ignoring the temporal changes over a 10-year time span. Working independently with the WOCE CFC data, Willey *et al.* [2004] reached the same conclusion. The radiocarbon maps could not be produced using these rules due to a lack of WOCE era data in the Atlantic; there were no data in the

northeast Atlantic and only one sparsely sampled cruise in the South Atlantic. Therefore the Atlantic radiocarbon maps ($\Delta^{14}\text{C}$ and bomb-produced ^{14}C) were constructed with data from the 1980s (primarily TTO and SAVE) results. The SAVE sampling occurred November 1987 to March 1989, so the time mismatch with WOCE is small; however, the North Atlantic is approximately a decade out of phase. Additional radiocarbon samples collected in the North Atlantic are currently being analyzed. When these results are final, the radiocarbon maps for the North Atlantic will be updated.

[26] The first step of the mapping procedure was to interpolate the discrete data onto the depth surfaces. For this work the data at each station were fit with a smooth curve (quasi-Hermitian- piecewise polynomial) that was then evaluated at 33 surfaces. Each interpolated value was subjected to a “distance to nearest data” criterion. The severity of the rejection criterion relaxed with depth. Specifics are given in Appendix A, Table A2 in section A7, and Appendix B. No extrapolation was allowed. Testing implies that this smooth curve interpolation is marginally better than linear interpolation and roughly comparable in computation time. This algorithm is not subject to the ringing associated with many spline fitting routines.

[27] The horizontal mapping resolution was 1° (latitude by longitude). Both the horizontal grid box edges and the depth surfaces were chosen to match existing climatological data sets (work by *Conkright et al.* [2002] and its predecessors). The horizontal gridding of the discrete data used the objective analysis procedure described by *Sarmiento et al.* [1982] that was based on the work of *Gandin* [1963]. Other than the error estimation, the procedure is very similar to that described by *LeTraon* [1990]. For all the maps a value of 0.1 was used for the input “noise” parameter. For map surfaces from 0 to 3500 m the correlation length scales were 1550 km east to west and 740 km north to south [*Kawasi and Sarmiento*, 1985, 1986]. Surfaces below 3500 m used 740 km for both directions. This change reduced the influence of data located beyond topographic boundaries, that is, across ocean ridges. In the deep Atlantic, where this problem can be significant, the eastern and western basins were mapped independently. The length scales used, combined with the low data density, result in significant smoothing in all high gradient regions. The objective analysis calculation produces an error estimate in addition to the estimated field.

[28] Primarily due to computer limitations, the Atlantic, Indian, and Pacific were mapped independently. At high southern latitudes, each ocean was “extended” both eastward and westward to facilitate subsequent merging into a global map (see Figure 10 in section 5.3 for an example of the extension used in the Pacific maps). A fourth set of maps was produced covering the entire Southern Ocean with the wintertime outcrop of the 17° isotherm used as the northern boundary. Finally, for each property at each surface, the four ocean maps were pasted together to yield a global picture. For those grid boxes where ocean maps overlapped, the individual grid box values were smoothed by computing an error weighted average and standard error. An exception to these rules was used for the radiocarbon and bomb-radiocarbon maps. For these tracers

the data set was small enough that the entire global ocean could be mapped at once for each surface. The reduced data density also required increasing the east-west correlation length scale to 2500 km for the upper surfaces (0–3500 m). Bomb-radiocarbon maps were calculated only for the upper 1500 m of the water column. Below that depth the signal is too small to produce reliable results with this procedure.

[29] Once the maps were completed, the resulting property and error fields were transferred to CDIAC and translated into netCDF format (see <http://www.unidata.ucar.edu/packages/netcdf/>). CDIAC provides a Live Access Server (<http://cdiac3.ornl.gov/las/servlets/dataset>; for information on LAS, see http://ferret.pmel.noaa.gov/Ferret/LAS/ferret_LAS.html) that can be used to view the mapped data either as surfaces or sections. Alternately, entire data blocks (netCDF, ASCII or ODV) can be downloaded and manipulated locally using Ferret (see <http://ferret.pmel.noaa.gov/Ferret/>) or similar software. R. Schlitzer translated the gridded files into ODV format (http://www.awi-bremerhaven.de/GEO/ODV/data/GLODAP-v1.1_gridded/index.html).

5. Discussion

5.1. Parameter Distributions

[30] The number of parameters considered combined with the global nature of this project makes even a brief description of the three-dimensional distributions difficult. As noted, some of these results have already been published. Given the scope of this project, the publications to date and the fact that those publications have generally used summary quantities, integrals, and/or vertical sections, and the publications expected in the near future, we restrict this presentation to a very limited selection of maps, mean profiles, and inventories. For the steady state tracers (TA and potential alkalinity) and those that have easily measurable concentration throughout the water column (DIC, $\Delta^{14}\text{C}$) we show distributions on the 0 m, 1200 m, and 3500 m surfaces. For anthropogenic tracers (anthropogenic CO_2 , bomb- ^{14}C , pCFC-11 and pCFC-12), depths are restricted to the thermocline, 0 m, 500 m and 1000 m. Chlorofluorocarbon partial pressure maps are shown rather than concentration maps because the latter are so strongly influenced by the solubility temperature dependence. In Figures 2–5 the three maps for each tracer have the same color scale. This choice reduces the detail for each map, but allows one to compare concentration differences between the surfaces. Constant interval contour lines without labels were added to each image to help visualize the large-scale property gradients. High-quality versions of these maps and myriad others as well as zonal and meridional sections are easily obtained by downloading the gridded products and presenting the results with GMT [*Wessel and Smith*, 1991, 1996, 1998] or similar software. Moderate quality output is available from the GLODAP LAS at CDIAC. The station locations used to produce each map of each property are available as part of the ASCII gridded data “tar” files at CDIAC (http://cdiac.ornl.gov/ftp/oceans/GLODAP_Gridded_Data/).

[31] Figure 2 shows TA and DIC concentration maps. The surface TA distribution closely resembles salinity [*Conkright et al.*, 2002] with maximum values generally

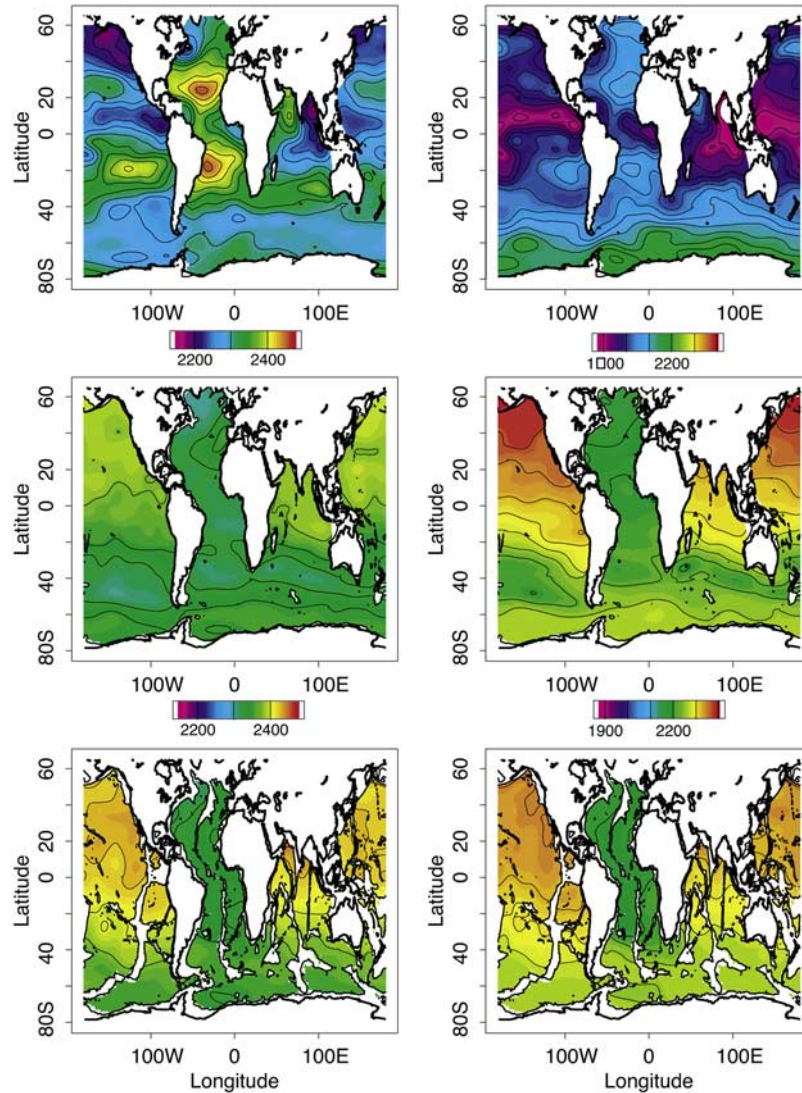


Figure 2. Objective maps of (left) TA ($\mu\text{mole/kg}$) and (right) DIC ($\mu\text{mole/kg}$) on the (top) 0 m, (middle) 1200 m, and (bottom) 3500 m surfaces. Unlabeled contours at an interval of $25 \mu\text{mole/kg}$ are included to help discern gradients. For each parameter the color scale is the same for all three subplots to help visualize vertical trends. Individual maps with significantly more detail are available from the website ([http://cdiac3.ornl.gov/las/servlets/data set](http://cdiac3.ornl.gov/las/servlets/data%20set)).

found in the subtropical gyres, particularly in the Atlantic. Like salinity, surface alkalinity is strongly controlled by net evaporation-precipitation and mixing. The correlation between surface salinity and alkalinity is so strong that salinity usually can be used as a reasonable surface alkalinity proxy [Millero *et al.*, 1998b]. One area where the surface alkalinity correlation with salinity breaks down is the Southern Ocean. There, TA values are enriched relative to salinity. This enrichment reflects upwelling of deep waters that have accumulated TA from the dissolution of calcium carbonate. Upwelling near the equator also increases TA relative to salinity, particularly in the Pacific.

Neither of these features is apparent in the surface TA distribution map given here because of the broad color scale; however, both are clearly depicted in the LAS version.

[32] The surface DIC distribution is affected by physical processes; however, the pattern is more similar to the nutrients (e.g., phosphate) than to salinity. This is because DIC concentrations are more strongly affected by biology than is TA [e.g., Murnane *et al.*, 1999; Sabine *et al.*, 1995]. Like the nutrients, DIC values are enriched in the Southern Ocean relative to salinity. The decrease in concentrations as one moves equatorward across the polar and subantarctic

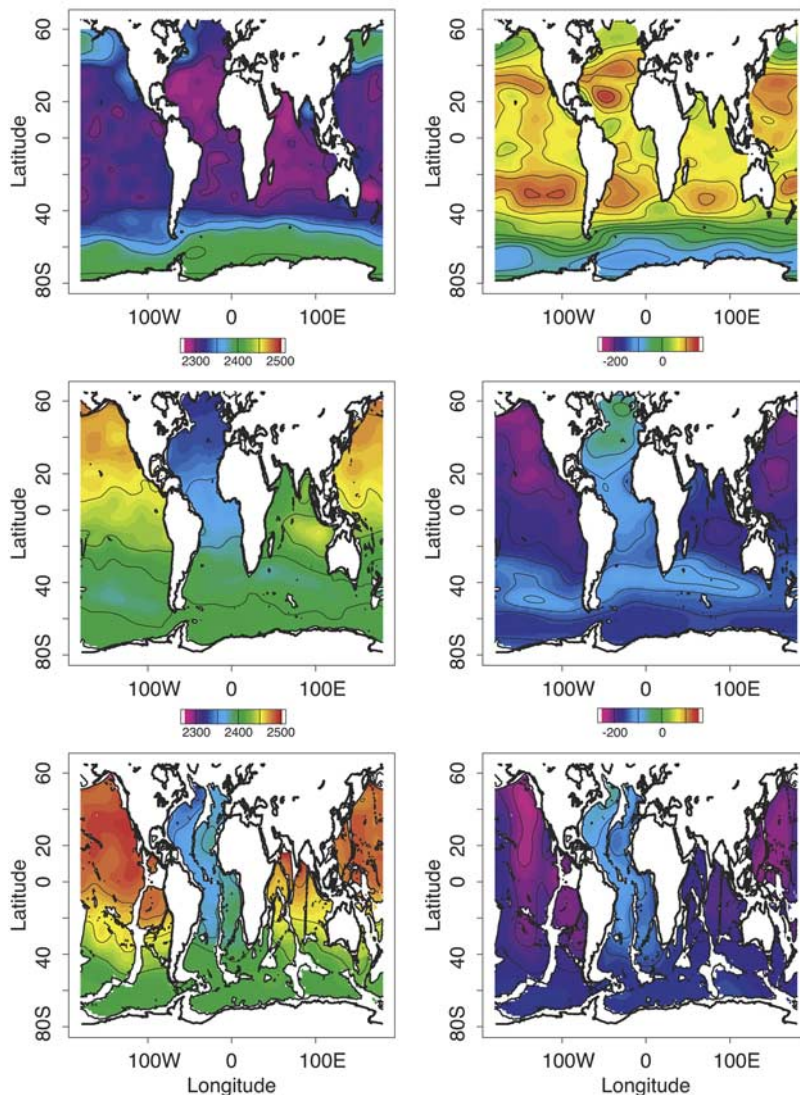


Figure 3. Objective maps of (left) potential alkalinity ($\mu\text{mole/kg}$) and (right) $\Delta^{14}\text{C}$ (‰) on the (top) 0 m, (middle) 1200 m, and (bottom) 3500 m surfaces. Unlabeled contours at an interval of 25 $\mu\text{mole/kg}$ are included to help discern gradients. For each parameter the color scale is the same for all three subplots to help visualize vertical trends. Individual maps with significantly more detail are available from the website (<http://cdiac3.ornl.gov/las/servlets/data set>).

fronts, however, is not as dramatic for DIC as for the nutrients because of the effects of mixing and gas exchange on DIC. The equatorial zone has the lowest surface DIC value in each basin, and the equatorial Pacific is significantly lower than the equatorial Atlantic. The surface Bay of Bengal is markedly lower than the surface Arabian Sea. This difference is consistent with the phosphate and salinity distributions.

[33] At depth, the TA and DIC distribution patterns are dominated by the influence of large-scale circulation. At 1200 m and 3500 m the TA and DIC concentrations are relatively uniform in the Atlantic, but show substantial south to north gradients in the Indian and Pacific. The 1200-m DIC gradients are greater than those for TA reflecting the shallower remineralization length scale of

organic carbon relative to calcium carbonate. In the North Atlantic at 1200 m the DIC distribution contains a minor contribution from anthropogenic CO_2 . The thermohaline circulation causes subtle patterns that are not apparent in the figure due to the color scale, but that can be seen in the online versions. For example, at 3500 m the North Atlantic western basin is significantly lower in TA than the eastern basin, reflecting the greater age of the eastern basin waters [Schlitzer, 1987]. This difference is also significant in the mean value from the bottle data (3500 m to bottom; mean, standard deviation, and standard error from bottle data; not volume weighted: western basin 2335, 13, 0.4; eastern basin 2351, 7, 0.4).

[34] The bottle data results were also used to calculate the aragonite and calcite saturation fraction for each sample

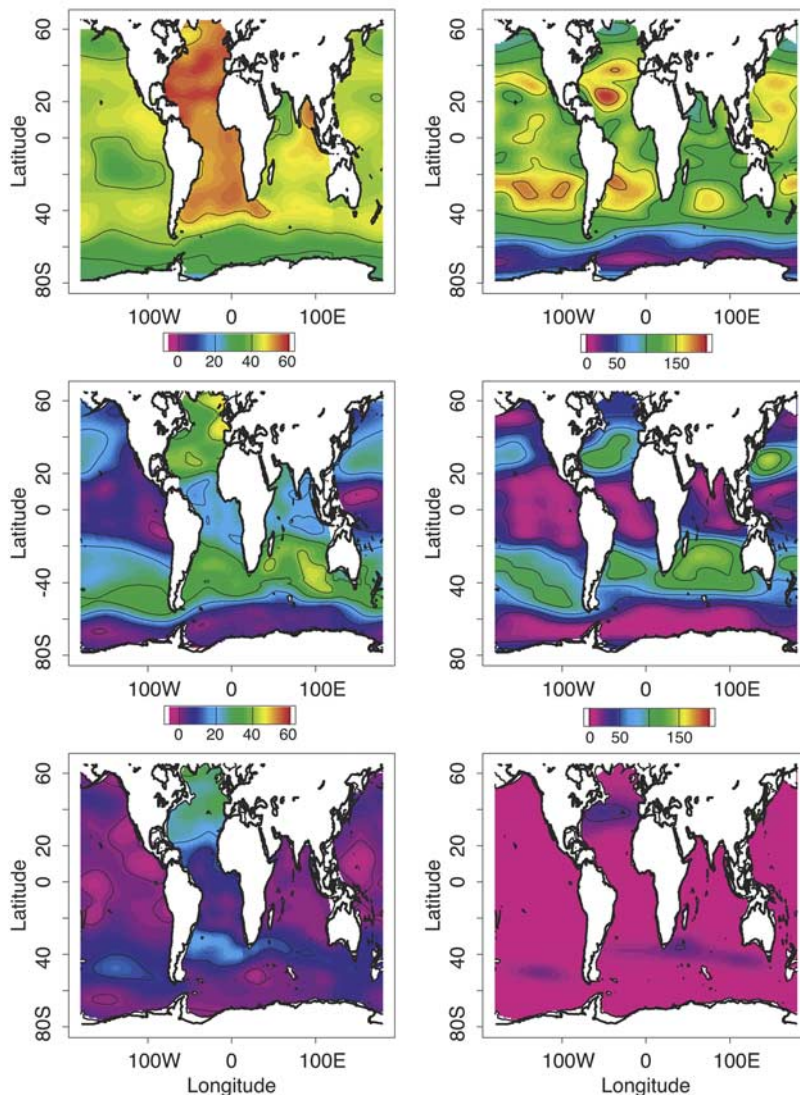


Figure 4. Objective maps of (left) anthropogenic CO₂ (μmole/kg) and (right) bomb-Δ¹⁴C (‰) on the (top) 0 m, (middle) 500 m, and (bottom) 1000 m surfaces. Unlabeled contours at an interval of 10 μmole/kg for anthropogenic CO₂ and 25‰ for bomb-Δ¹⁴C are included to help discern gradients. For each parameter the color scale is the same for all three subplots to help visualize vertical trends. Individual maps with significantly more detail are available from the website ([http://cdiac3.ornl.gov/las/servlets/data set](http://cdiac3.ornl.gov/las/servlets/data%20set)).

having both TA and DIC values. At each station the equilibrium saturation depth was determined using the previously described constrained vertical interpolation scheme. Those depths were then objectively mapped and the results presented by Feely *et al.* [2004, Figure 2]. There is pronounced shoaling of both the aragonite and calcite saturation depth from the Atlantic through the Indian to the Pacific because of the higher DIC/TA ratios in the intermediate and deep waters of the Indian and Pacific relative to the Atlantic. Large-scale enrichment of DIC relative to TA is caused by respiration processes as the water circulates along the deep conveyor belt [Broecker, 2003]. In the far

North Pacific the aragonite and calcite saturation horizons shoal to approximately 200 m and 1000 m, respectively. Carbonate chemistry in this region is also impacted by anthropogenic CO₂ [Feely *et al.*, 2002]. Surprisingly, however, portions of the northern Indian Ocean and eastern equatorial Atlantic Ocean are also undersaturated with respect to aragonite at shallow depths. The Atlantic undersaturation region appears to be increasing in areal extent as a consequence of anthropogenic CO₂ accumulations [Lee *et al.*, 2003; Chung *et al.*, 2003, 2004].

[35] Figure 3 shows potential alkalinity and Δ¹⁴C distribution maps. Potential alkalinity ((TA + Nitrate) × 35/Salinity)

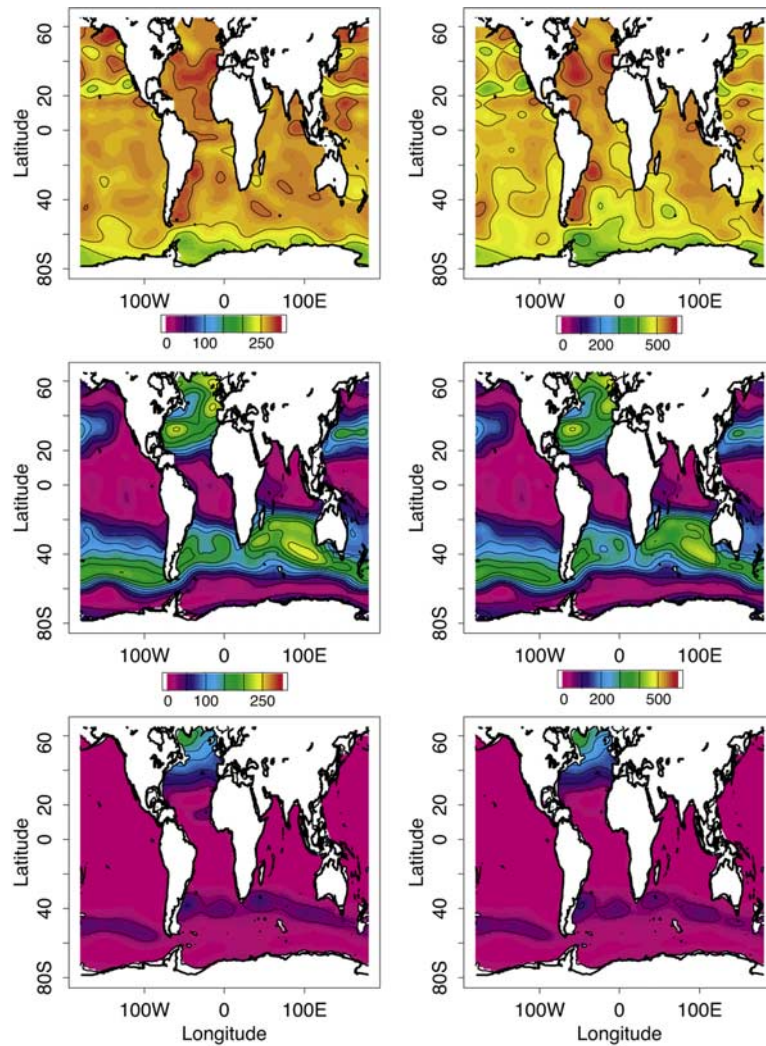


Figure 5. Objective maps of (left) pCFC-11 (patm) and (right) pCFC-12 (patm) on the (top) 0 m, (middle) 500 m, and (bottom) 1000 m surfaces. Unlabeled contours at an interval of 25 patm for pCFC-11 and 50 patm for pCFC-12 are included to help discern gradients. For each parameter the color scale is the same for all three subplots to help visualize vertical trends. Individual maps with significantly more detail are available from the website (<http://cdiac3.ornl.gov/las/servlets/data> set).

corrects TA for the effects of mixing and small changes resulting from the decomposition of organic matter, leaving only the influence of calcium carbonate dissolution [Brewer and Goldman, 1976]. Consequently, potential alkalinity increases with depth everywhere; however, the top to bottom gradient is weakest in the Southern Ocean and strongest in the Pacific and Indian. Surface potential alkalinity is relatively constant between 50°N and 40°S – 50°S , reflecting the strong TA-salinity correlation. The surface potential alkalinity distribution highlights the relatively enriched TA values in the Southern Ocean discussed with the previous figure. Elevated surface values in the western subpolar North Pacific reflect the fact that the carbonate saturation horizons are shallow in this region and deep winter convection can mix up higher potential alkalinity values [Sarmiento *et al.*, 2004]. The deep water potential alkalinity distribution is dominated by large-scale circula-

tion and by shoaling of the carbonate saturation depth [Feely *et al.*, 2004]. The intermediate and deep distributions are affected by alkalinity accumulation from calcium carbonate dissolution as the waters move from the North Atlantic to the Indian and Pacific. In the Atlantic at 1200 m the meridional potential alkalinity gradient is significantly greater than for TA.

[36] The surface $\Delta^{14}\text{C}$ distribution is strongly influenced by uptake of bomb produced ^{14}C from the atmosphere. The equilibration time for this process is approximately 10 years; therefore, the long residence time of surface water in the subtropical gyres influences the surface $\Delta^{14}\text{C}$ distribution. Equilibrium dynamics (temperature) favor uptake in the Southern Ocean; however, rapid vertical mixing and consequently short surface water residence times dilute the values there. The intermediate and deep $\Delta^{14}\text{C}$ distributions reflect aging of the waters along the

path of the large-scale circulation, with contamination at some intermediate depth locations from deep injection of bomb ^{14}C . As noted by *Rubin and Key* [2002], there is a very strong linear relationship between the increase in potential alkalinity and natural ^{14}C decay in the deep ocean. Since the deep $\Delta^{14}\text{C}$ reflects the aging of the waters, the global carbonate dissolution rate in deep waters must be relatively uniform. Deep radiocarbon also correlates strongly with AOU implying a near constant oxygen utilization rate of approximately $0.1 \mu\text{mol kg}^{-1} \text{yr}^{-1}$ [Key, 2001]. $\Delta^{14}\text{C}$ generally decreases with depth. The weakest vertical gradients are in the Southern Ocean and the strongest are in the Indian and Pacific. Significant detail exists in both the bottle data and gridded results which are not shown here. For example:

[37] 1. As with alkalinity, the deep western North Atlantic $\Delta^{14}\text{C}$ is significantly higher than the eastern North Atlantic with the difference deriving from the ventilation pathway [Schlitzer, 1987; Matsumoto and Key, 2004, Figure 1].

[38] 2. The deep water near bottom $\Delta^{14}\text{C}$ distribution very clearly shows water mass aging along the abyssal circulation pathway from Atlantic to Indian to Pacific [Matsumoto and Key, 2004, Figure 3].

[39] 3. In the near-bottom Pacific the northward abyssal flow is concentrated in a western boundary current centered approximately on the date line in the Southern Hemisphere and veering westward north of the equator [Schlosser et al., 2001, Plate 5.8.17, p. 428]. Recently, Roussenov et al. [2004] used an isopycnal coordinate Pacific Ocean model to investigate how bottom water transport and diapycnic mixing determine the deep and abyssal radiocarbon distribution. They found that relatively fast lateral transport of bottom waters control the horizontal distribution while a balance between advection-diffusion and decay control the vertical distribution. They also found that the distribution was rather sensitive to the influence of bottom topography. They did not consider the influence of particulate matter; however, this issue was addressed recently by Srinivasan et al. [2000] in an Indian Ocean study based on GEOSECS results.

[40] 4. The conventional radiocarbon age at 3500 m ranges from ~ 400 years in the northwest Atlantic to ~ 2200 years in the subtropical to subpolar North Pacific.

[41] 5. The southward flow of North Pacific Deep Water at approximately 2500 m is focused into two core regions, with one centered near 160°W and the other adjacent to South America [Schlosser et al., 2001, Plate 5.8.18, p. 446].

[42] 6. The oldest water in the ocean (lowest radiocarbon) is in the North Pacific at a depth of approximately 2200 m. Contrary to what one might have assumed from the GEOSECS data, the oldest values are not adjacent to the Aleutian slope but are displaced southward. This implies a deep ventilation pathway, presumably in a zonal flow, which is north of the deep radiocarbon minimum area.

[43] Figure 4 shows anthropogenic CO_2 and bomb- ^{14}C distributions in the thermocline. Unlike the measurements described so far, these two tracers are derived. Although both are anthropogenic carbon tracers, their atmospheric histories and equilibration times are very different. Anthropogenic CO_2 has been exponentially increasing in the

atmosphere for over 200 years and has an average air-sea equilibration time of about 1 year. The bomb-produced radiocarbon history in the atmosphere is a spike beginning in 1955, reaching maximum in mid-1960s, and subsequently decaying exponentially. As with naturally occurring $\Delta^{14}\text{C}$, the atmosphere-surface ocean equilibration time is approximately 10 years. Consequently, surface ocean concentrations lag the atmosphere significantly [Key, 2001].

[44] Anthropogenic CO_2 concentrations are almost always highest at the surface and decrease with depth. Along an isopycnal, concentration decreases with distance from the outcrop of that density surface. The lowest surface values are found in the Southern Ocean. The most dramatic feature of the surface ocean anthropogenic CO_2 distribution is the relatively high value throughout the Atlantic. We were surprised by the magnitude of the difference and do not yet understand it. A slightly different function was used for the Atlantic surface anthropogenic CO_2 estimates (compare Sabine et al. [1999, 2002a] with Lee et al. [2003]), but tests have indicated that this cannot explain the difference. The fact that the Atlantic sector of the Southern Ocean is consistent with the other Southern Ocean sectors also argues against this explanation. Higher surface Atlantic concentrations are consistent with several factors (alkalinity, salinity, Revelle factor), but none of these is sufficient to explain the basin to basin difference. Relative to the other oceans, the Atlantic WOCE era carbon data were somewhat problematic [Wanninkhof et al., 2003]. We are currently expanding the Atlantic data set substantially in order to investigate this issue, but we do not currently believe that the input data (i.e., the measurements) pose any significant problem. The Atlantic offset is approximately the same as the stated uncertainty for the surface anthropogenic CO_2 estimates. McNeil et al. [2003] estimated anthropogenic CO_2 accumulation in the ocean for the period 1980–1999 based solely on CFC ages. While not totally comparable to the estimates given here, they found surface Atlantic accumulations to be almost the same as surface Pacific accumulations (see their Figure 4). For the present, we accept the difference as real and will try to understand it with further work. The Bay of Bengal surface waters also have high surface anthropogenic CO_2 estimates. These surface waters are strongly influenced by riverine input [Sabine et al., 1999], and perhaps this is also important in the Atlantic.

[45] The 500-m surface shows where intermediate waters penetrate the ocean interior. The 1000-m surface in Figure 4 has discernible anthropogenic CO_2 concentrations only in the North Atlantic where North Atlantic Deep Water is transporting it into deeper waters. Significantly more detail on these surfaces can be found in the original papers [Sabine et al., 1999, 2002a; Lee et al., 2003], and the global summary [Sabine et al., 2004].

[46] The bomb ^{14}C distribution in Figure 4 is similar to anthropogenic CO_2 , but there are important differences. Most prominent, the Atlantic surface values are not anomalous relative to the Pacific and Indian. In surface waters, relatively high bomb ^{14}C values are found in the subtropical gyres of each ocean. This reflects the stability, or relatively long residence time, of these waters. The

intermediate water bomb ^{14}C distribution is very similar to anthropogenic CO_2 . At 1000 m the bomb ^{14}C distribution is more restricted than that of anthropogenic CO_2 , but occurs at similar locations. The 1000-m bomb ^{14}C signal is easily visible only in a narrow band at the northern edge of the Southern Ocean and in the North Atlantic. Rather than trying to quantify the bomb ^{14}C signal, *Östlund and Rooth* [1990] described the change in the measured radiocarbon distribution in the North Atlantic between GEOSECS (1972) and TTO (1983). A similar change exists between TTO and WOCE. Small but measurable changes are found in the North Atlantic deep western boundary current at least as far south as the Lesser Antilles. These deep changes are best investigated by manual examination of the data rather than computer gridding. A weak bomb ^{14}C signal exists at 1000 m in the far northwest Pacific adjacent to the formation region for North Pacific Intermediate Water.

[47] Figure 5 shows pCFC-11 and pCFC-12 on the three depth surfaces. These distributions look very similar to the other anthropogenic tracers. Like the bomb ^{14}C , the CFCs have a shorter atmospheric history than anthropogenic CO_2 . Unlike the bomb ^{14}C , CFCs have an equilibration time of weeks, much shorter than anthropogenic CO_2 . The only clear pattern in the surface ocean pCFC distribution is relatively low values adjacent to Antarctica. North of the Southern Ocean the distributions have no pattern that makes sense in the context of what is known about upper thermocline-surface ocean circulation. For the major oceans the surface values are essentially equilibrium values and the patterns are more likely indicative of the combined errors resulting from different sampling times and the mapping procedure. At the 500-m and 1000-m levels the maps for pCFC-11 and pCFC-12 show virtually identical trends, differing only in scale. At 500 m in the Southern Hemisphere, intermediate and mode waters have high values which decrease northward. For both tracers the highest values at 500 m occur in the Indian Ocean southwest of the southwestern tip of Australia. A similar band of high values exists in the North Pacific. The entire North Atlantic has significant values at 500 m; however, rather than being a band of concentration, the distribution is reminiscent of that described for tritium in earlier works [e.g., *Sarmiento*, 1983; *Jenkins*, 1998]. That is, interior ventilation appears to be along isopycnals with the primary entry point toward the northeastern portion of the subtropical gyre. At 1000 m the same patterns are present, except the North Pacific signal is too weak to show in the plots. The North Atlantic pattern has the same shape as at 500 m, but the spatial extent is reduced. The Southern Ocean band is significantly narrower than at 500 m.

[48] The data were also used in a recent data-model comparison [*Matsumoto et al.*, 2004]. They found that the models that successfully simulated the correct Circumpolar Deep Water $\Delta^{14}\text{C}$ and CFC-11 inventories tended to simulate higher anthropogenic CO_2 inventories than the data-based estimates. Much of the discrepancy was due to Pacific Ocean differences. It was not clear whether the discrepancy was due to model inadequacy or to the anthropogenic CO_2 estimation method.

[49] Figures 6 and 7 show mean ocean profiles calculated from the gridded property maps. Each datum is volume weighted. The Atlantic (circles, black), Indian (triangles, red) and Pacific (plus signs, blue) are defined to extend northward from the southern local wintertime outcrop of the 17°C isotherm (see bottom right panel of Figure 6 for outcrop location) to approximately 65°N , with longitudinal breaks south of Patagonia, Capetown, South Africa, and Hobart, Australia. The Southern Ocean (crosses, green) is defined as everything south of the wintertime outcrop of the 17°C isotherm.

[50] The profile shapes are dominated by large-scale thermohaline circulation coupled with air-sea gas exchange, and biological production and subsequent remineralization. There are a number of points worth mentioning.

[51] 1. The deep and bottom water concentrations (ages for ^{14}C) increase from Atlantic to Southern to Indian to Pacific Ocean.

[52] 2. At 800–1200 m all the profiles in Figure 6 show a relative extreme in the Atlantic for Antarctic Intermediate Water.

[53] 3. At 2000–3000 m all the Pacific profiles in Figure 6 show a broad relative extreme for North Pacific Deep Water.

[54] 4. The surface Atlantic alkalinity value is substantially higher than for the other oceans. This reflects the strong alkalinity:salinity correlation as indicated by the fact that the Atlantic surface potential alkalinity is not anomalous.

[55] 5. The Southern Ocean surface potential alkalinity is substantially higher than for the other oceans, reflecting upwelling of relatively old deep waters which are enriched due to carbonate dissolution.

[56] 6. The deepest Atlantic potential alkalinity datum appears to be anomalous. This may be due to the relative importance of Antarctic Bottom Water. This low potential alkalinity value forces the corresponding natural radiocarbon value to be high while the measured radiocarbon value is low. This apparent discrepancy requires further research, but may indicate a locally significant problem with the global radiocarbon separation algorithm [*Rubin and Key*, 2002].

[57] 7. In the Southern Ocean, natural radiocarbon has a distinct negative gradient from ~ 1500 m to the bottom, while the measured values are extremely uniform ($\sim -160\text{‰}$). If correct, this difference implies that dissolution of bomb ^{14}C contaminated carbonate particles is an unexpectedly large radiocarbon source in deep Southern Ocean waters (see *Fiadeiro* [1982] for a discussion of this topic in the Pacific, and see *Srinivasan et al.* [2000] for a similar consideration in the Indian).

[58] 8. Southern Ocean surface waters have substantially lower radiocarbon (measured and natural) than the other basins.

[59] 9. The surface Southern Ocean CFC-11 and CFC-12 concentrations are highest while the partial pressures are slightly lower than the other oceans. This difference is a clear demonstration of the strong solubility dependence on temperature. The Southern Ocean surface pCFC values indicate a small but statistically significant undersaturation. This is consistent with Figure 5, where it was shown that surface pCFC decreases significantly with increasing latitude in

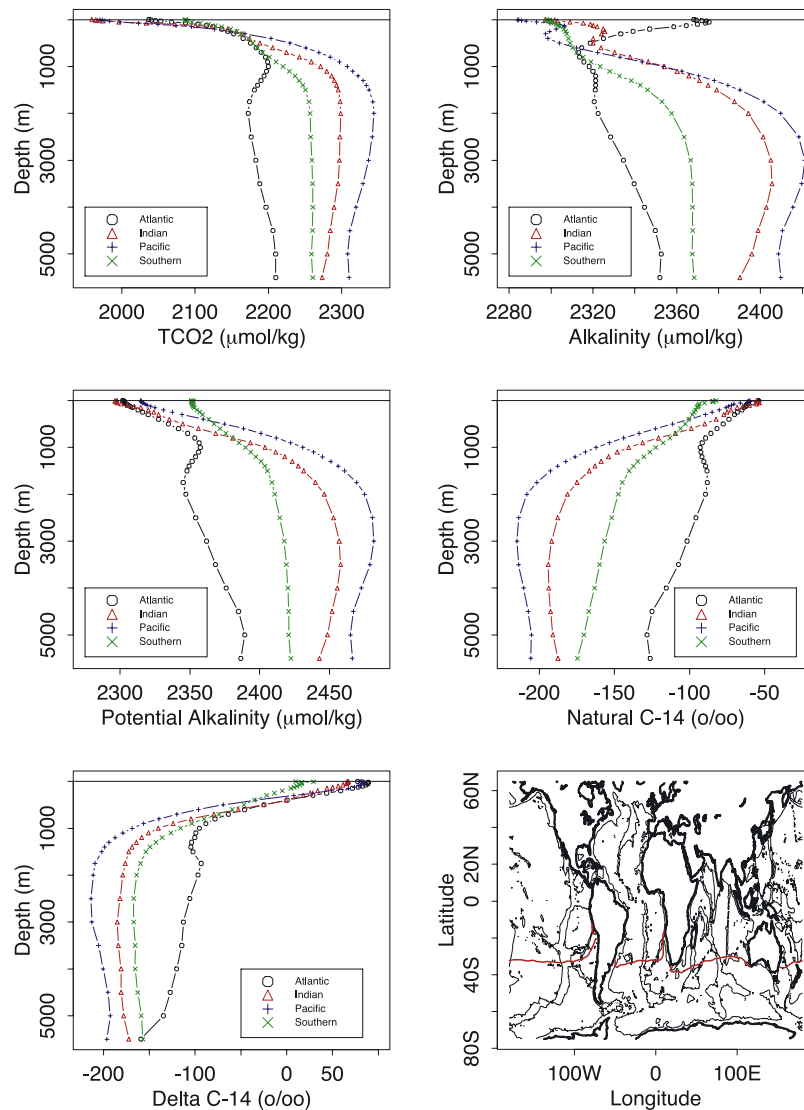


Figure 6. Average profiles with the data segregated by ocean. See text for discussion and data limits used. The averages are volume weighted and calculated from the gridded results. The bottom right panel shows the local wintertime outcrop of the 17°C isotherm, which was used as the boundary between the Southern Ocean and the other ocean basins.

the Southern Ocean surface and intermediate waters. CFC undersaturation in Southern Ocean surface waters has implications for the anthropogenic CO₂ calculation.

[60] 10. At 400–1000 m CFC partial pressures (and concentrations) are significantly lower in the Pacific than in the other oceans, implying a longer average ventilation time for the Pacific at these depths. The same pattern is seen for anthropogenic CO₂. At these depths bomb ¹⁴C is lowest in the Pacific, but only marginally. One possible interpretation is that carbonate dissolution has a more significant influence on the radiocarbon depth distribution in the Pacific than elsewhere, but this has not been investigated yet.

[61] 11. All of the anthropogenic parameters show a finite mean value at 1600 m in the Atlantic that is due primarily to tracer incorporation into North Atlantic Deep

Water. The data distribution is such that the various parameter maps do a poor job of capturing the deep western boundary currents, particularly in the North Atlantic.

[62] 12. The surface bomb radiocarbon is significantly lower in the Southern Ocean than the other oceans. This is because Southern Ocean waters do not remain at the surface long enough to attain equilibrium [Toggweiler and Samuels, 1993] and/or the flux into the Southern Ocean is diluted by deep mixed layers.

[63] 13. In the Atlantic and Pacific Oceans the bomb radiocarbon maximum is clearly subsurface (see Key [2001] for a brief discussion).

5.2. Inventories

[64] Global inventories were calculated for DIC, TA, CFC-11, CFC-12, anthropogenic CO₂, bomb radiocarbon,

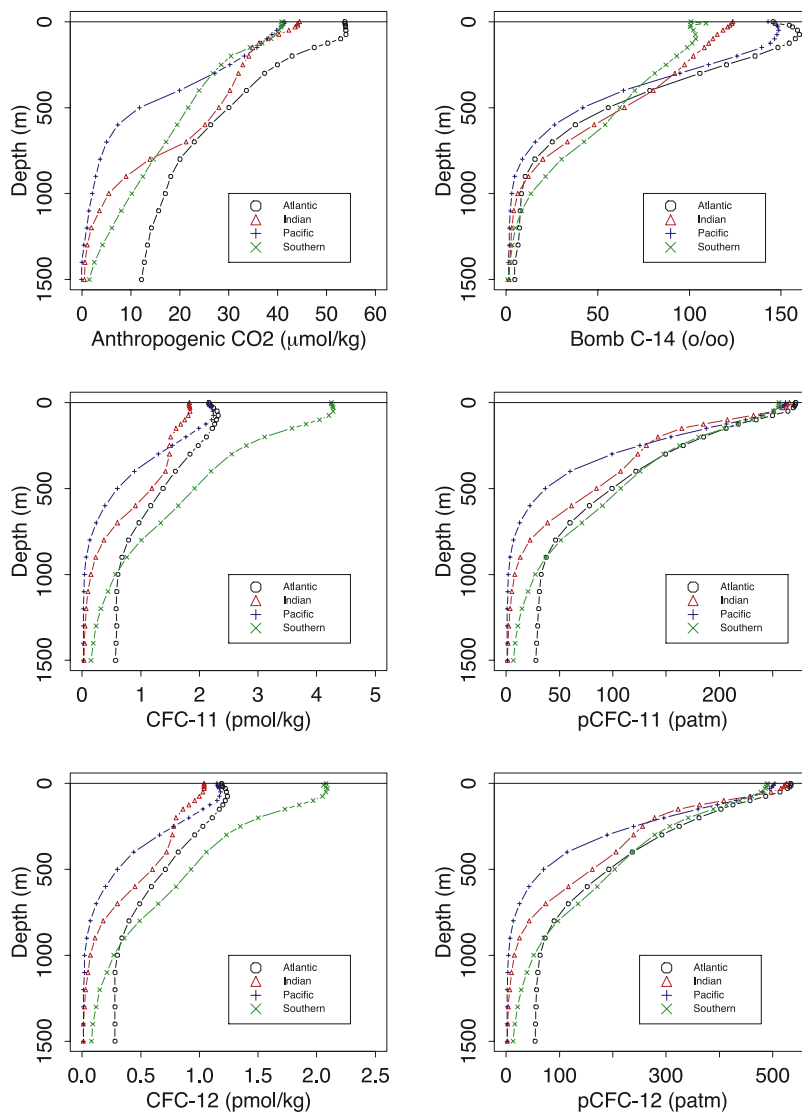


Figure 7. Average profiles with the data segregated by ocean. See text for discussion and data limits used. The averages are volume weighted and calculated from the gridded results.

and natural radiocarbon. For bomb and natural radiocarbon the individual values were converted to atoms per volume, and those values were mapped prior to integration. The bomb radiocarbon integration was limited to the upper 1600 m, but the others extended over the entire water column. The results of these integrations are in Table 1.

[65] The anthropogenic CO₂ integration is identical to that described by *Sabine et al.* [2004], but they also extended the estimate using proxy tracers to include the Arctic Ocean and marginal seas. The anthropogenic CO₂ inventory amounts to an increase of only 0.3% in the natural inventory while the bomb radiocarbon addition is about 2%. The CFC-11 integration is remarkably similar to that presented by *Willey et al.* [2004]. They used a similar data set, but a significantly different mapping/integration procedure in which the data at each station was vertically integrated, then those values were horizontally mapped. They reported an inventory of 5.5×10^8 moles compared to our result of 5.4×10^8 moles. Their integration included an

estimate of 2.8×10^7 moles for the Arctic Ocean that ours does not have. In spite of the fact that these two estimates are almost identical, we estimate that the uncertainty for each inventory in Table 1 is approximately 15%. This error estimate is an educated guess. The uncertainties in the objectively mapped values are highly correlated both vertically and horizontally, so normal error propagation cannot be used.

[66] *Broecker et al.* [1995] estimated a global bomb radiocarbon inventory of 3.29×10^{28} atoms using the silicate separation method and the combined GEOSECS, TTO, and SAVE data sets. When the uncertainties in the estimates are considered, their inventory is identical to that derived here (3.13×10^{28} atom). The large-scale features shown in their inventory distribution maps (their Figures 11–14) were all apparent in this work. One would expect an increase in the ocean inventory over the time separating the two data sets, and, indeed, detailed comparisons at specific locations do show the expected increase.

Table 1. Global Inventories

Parameter	Global Integral ^a	Units
DIC	2.98×10^{18}	mole
TA	3.12×10^{18}	mole
Natural ^{14}C	1.79×10^{30}	atom
Bomb $^{14}\text{C}^b$	3.13×10^{28}	atom
Anthropogenic CO_2	8.82×10^{15}	mole
	1.06×10^2	PgC ^c
CFC-11	5.44×10^8	mole
CFC-12	2.72×10^8	mole

^a“Global” includes only those areas shown in the various surface property maps (Figures 2–5), that is, excluding the Arctic Ocean and all Mediterranean seas.

^bVertical integration stopped at 1600 m.

^cPetagrams (10^{15}g) carbon.

We attribute the similar inventories to chance and recognize that quantifying the decadal change requires a much more careful analysis which is currently in progress.

[67] Figure 8 shows the vertical column inventories for the anthropogenic tracers. Maps for the other parameters (TA, potential alkalinity, DIC, $\Delta^{14}\text{C}$, natural $\Delta^{14}\text{C}$) are not shown, since the inventory distributions are dominated by local water depth. Each inventory map has low values adjacent to Antarctica and in the tropics. The anomalously low inventory values for all four tracers along much of the east coast of the Americas is due to shallow water depth. The highest column inventory values for anthropogenic CO_2 and the CFCs are in the North Atlantic and reflect the relative importance of uptake into North Atlantic Deep Water. The North Atlantic bomb radiocarbon values are also

high, but equivalent inventories exist in the northwestern Pacific, indicating uptake into North Pacific Intermediate Water, and in a band centered near 35°S . The anthropogenic CO_2 and CFC maps also show elevated inventories in the south; however, these relative maxima are weak relative to the North Atlantic values.

[68] Comparison of the tracer inventory maps shows that the CFC Southern Hemisphere relative maximum is farthest south, followed northward by anthropogenic CO_2 and then bomb radiocarbon. For all four tracers the Southern Hemisphere relative inventory maximum extends farther north in the Indian than in the Pacific or Atlantic. The trend with latitude is better illustrated by comparing concentrations along a meridional section. Figure 9 shows bomb radiocarbon, anthropogenic CO_2 , and CFC-11 concentrations along WOCE section P16 ($\sim 152^\circ\text{W}$) in the eastern central Pacific. The section pattern is similar for all three tracers. The isolines are deepest in the gyre basins and shoal at the equator and toward the poles. To first order, the concentrations are consistent with the density distribution. The similarity in the concentration patterns among these sections implies that the meridional offset in the southern column inventory maxima noted for Figure 8 is primarily due to differences in the near-surface concentration distributions. The ordering is consistent with the air-sea tracer equilibration times: CFC (~ 2 weeks) $<$ CO_2 (~ 1 year) $<$ ^{14}C (~ 10 years). We currently assume that there is a causal relationship between the location of the southern inventory maxima and some combination of temperature, air-sea equilibration time, surface water

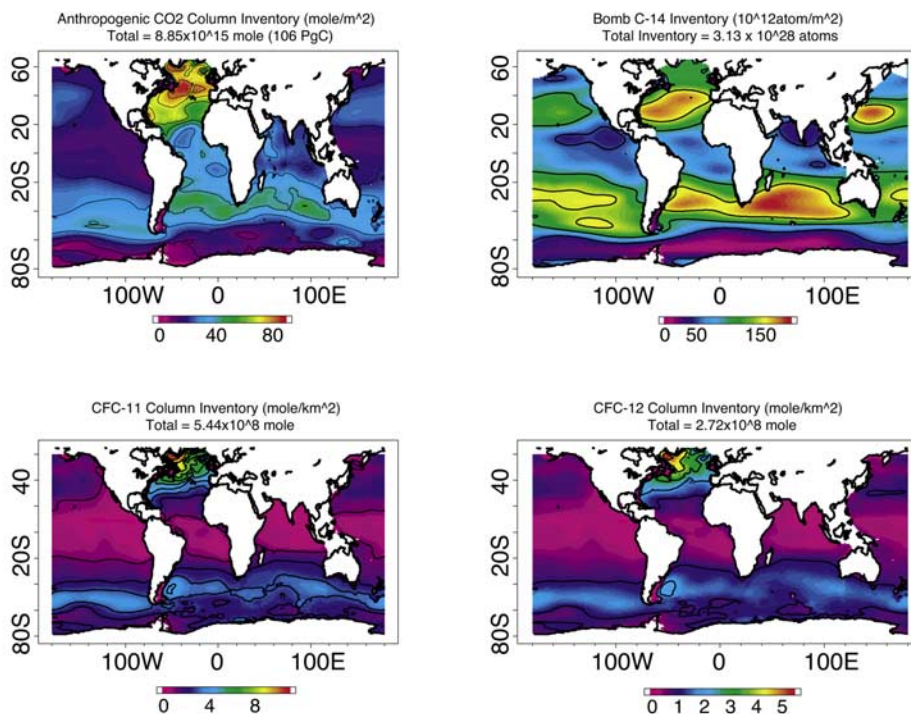


Figure 8. Vertical column inventories for the anthropogenic tracers included in this study. Note that the bomb radiocarbon is in atomic rather than permil units and that the bomb radiocarbon integration only covers the top 1600 m of the water column. The anthropogenic CO_2 and CFC inventories cover the entire water column.

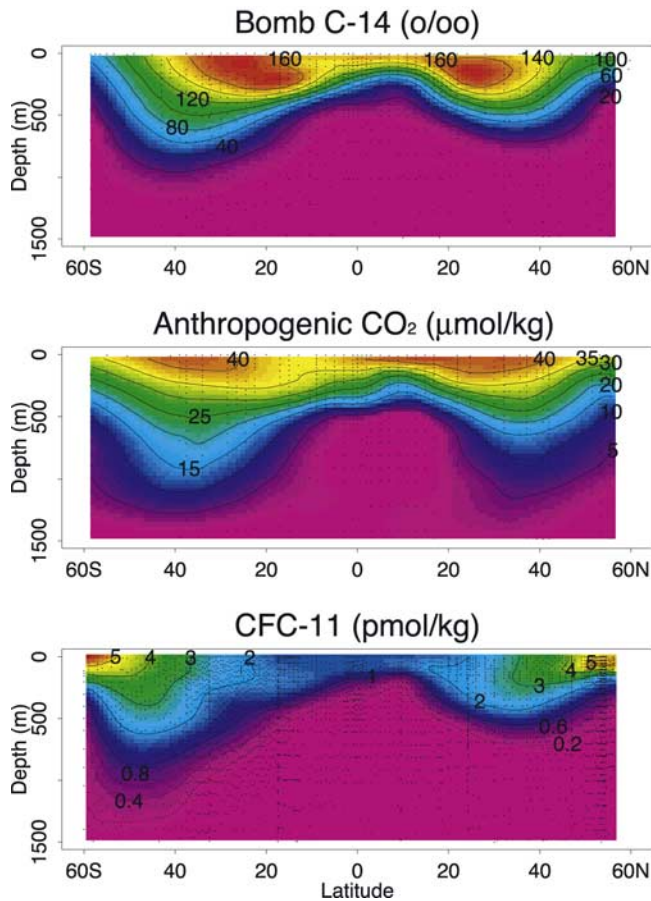


Figure 9. Vertical sections of bomb radiocarbon, anthropogenic CO₂, and CFC-11 concentrations along WOCE section P16 (~152°W) in the eastern central Pacific. The distributions are similar, but differences in the location of the near surface concentration maxima appear to be responsible for the dislocation of the southern hemisphere column inventory maxima (see text and Figure 8).

residence times, and intermediate water formation mechanisms and have begun to investigate these issues using numerical ocean models and water mass separation techniques.

5.3. Comparison to Previous Work

[69] Of the parameters considered here, only TA and DIC have previously been mapped globally. *Goyet et al.* [2000, and references therein] (hereinafter GHR) used a significantly different mapping procedure with a somewhat smaller set of cruises. In their method for alkalinity, they divided the water column into two zones: from the bottom of the wintertime mixed layer down to 1000 m and from 1000 m to the bottom. The TA measurements in each depth zone for each station were fit using

$$TA = a + b\Theta + cS, \quad (1)$$

where Θ and S are potential temperature and salinity. Once each station had been fit, the regression coefficients (a , b , c) were individually mapped onto a global grid using one of

the algorithms contained in the GMT software package [Wessel and Smith, 1998]. The mapped coefficients were then combined with climatological temperature and salinity data [Levitus and Boyer, 1994a, 1994b; Levitus et al., 1994] to produce the alkalinity fields. They estimated uncertainties for the Atlantic, Indian, and Pacific upper layer alkalinity as 4.6, 8.4, and 10.2 $\mu\text{mole/kg}$, respectively, and 5.9, 4.8, and 9.1 $\mu\text{mole/kg}$ for the deep layer. They estimated a global uncertainty below the mixed layer of 5.5 $\mu\text{mole/kg}$.

[70] GHR derived the DIC fields in a similar manner except that a single depth zone was used and each profile was fit using

$$DIC = a + b\Theta + cAOU + dS. \quad (2)$$

The DIC interpolation uncertainties were estimated using a limited Monte Carlo technique and were given as 8.1, 7.9, 14.5, and 9.4 $\mu\text{mole/kg}$ for the Atlantic, Indian, Pacific, and global oceans, respectively.

[71] Since this work and GHR both provide three-dimensional ocean distributions for DIC and TA that were based on similar input data, but substantially different mapping procedures, a brief comparison is warranted. This comparison cannot resolve which is more accurate, but can yield information on the error estimates and the different interpolation procedures. Since both estimates are on the same grid, a simple comparison can be obtained from the arithmetic difference. Figure 10 summarizes the differences for all the surfaces. Here we simply computed the difference for each grid cell, then averaged those differences for each map surface without volume weighting. The individual average differences are not particularly robust because the distribution of the differences was not normal in the statistical sense. For example, the average surface ocean alkalinity difference was 59 $\mu\text{mole/kg}$, while the median difference was 46 $\mu\text{mole/kg}$. To provide some scale against which the average difference can be judged, Figure 10 also shows the average of the error estimates for each surface derived from the GLODAP mapping procedure. As with the differences, these average errors are also prone to bias, in this case due to lack of independence rather than normality.

[72] In spite of the limitations, the summaries shown in Figure 10 appear to indicate systematic differences in the two products. In the upper kilometer the GLODAP TA values are considerably higher than the GHR values. Below 1 km the average TA difference changes sign and is only slightly larger than the average uncertainty predicted by the objective mapping procedure. The discontinuity in the difference profile at 1000 m is due to the TA data segregation and fitting procedure used by GHR. That is, their method did not force the two zone fitting procedure to be continuous near the interface separating the zones. The 1000-m discontinuity does not exist for DIC because GHR used a single function to fit the entire water column. Close investigation of the GHR estimates indicates a second discontinuity for each surface at 0° longitude. This discontinuity derives from the mapping procedure they used: The 0° longitude line was at the left and right edges of their maps, and no provision was made to force identical results at this longitude. For DIC the average difference between the two procedures shows a pattern with depth, but the

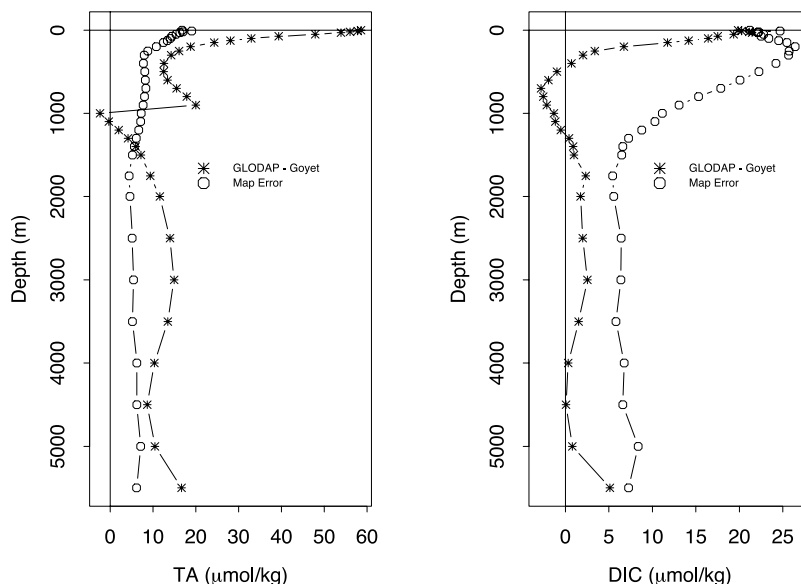


Figure 10. Summary difference (asterisks) for (left) TA and (right) DIC between the GLODAP mapping procedure and that used by GHR. For each surface the difference was computed for each grid cell, and a simple average was computed. The standard deviation of the average difference ranged from 14 to 56 for TA and from 11 to 46 for DIC, generally decreasing with depth. The discontinuity at 1000 m for TA is due to data segregation in fitting used by GHR. The open circles show the average estimated uncertainty for each surface from the objective analysis mapping method.

difference is less than the uncertainty predicted by the objective mapping calculation.

[73] We attempted to better understand the unexpectedly large alkalinity differences in the upper water column, but this effort provided only marginal information. Large differences were mostly limited to the Pacific. In the Pacific the largest positive differences were restricted to a band approximately 600–1000 km wide adjacent to the west coast of Central and North America. A broader band of large difference occurred in the western central Pacific. Large negative differences were restricted to the Bay of Bengal.

[74] Avoiding speculation, this comparison yields three concrete results: (1) There is a discontinuity in the GHR alkalinity field at 1000 m; (2) there is a discontinuity in the GHR TA and DIC fields at 0° longitude; and (3) the GHR error estimates, particularly for TA, are too small. Considering everything, we consider these differences to be rather minor and in fact recognize the significant potential of the GHR method. Their procedure uses information that we ignored, specifically the relatively well known distributions of temperature, salinity, and oxygen combined with the well-documented correlations which exist between DIC and TA, and common hydrographic parameters. Improved distribution maps might reasonably be expected by combining the GLODAP data and mapping procedure with the GHR data extrapolation method, but applying the GHR regressions horizontally on depth or density layers rather than vertically.

6. Conclusions

[75] GLODAP has produced calibrated uniform data files that should be of general value to the oceanographic community, particularly for studies of the carbon cycle.

The input data were limited to cruises that had “high-quality” measurements. Once compiled, these data were used to produce objectively mapped three-dimensional fields for the parameters of primary interest. The mapped fields were produced on the same grid used previously for temperature, salinity, oxygen, and nutrients. GLODAP is the largest ocean carbon compilation to date, but the data are still far too sparse to attempt a seasonal data segregation without resorting to some data expansion technique. Both the data and the mapped fields are therefore subject to the “summertime” seasonal bias generally found in similar products. All of the products of this effort are freely available electronically. We are hopeful that this compilation, which is denoted version 1.1, will be updated as data become available and omissions, errors, etc. are found and corrected. Future releases are also expected to include $^3\text{H}/^3\text{He}$ and focus on $\delta^{13}\text{C}$, which was included in this bottle data set but otherwise ignored.

Appendix A

A1. Database Construction Details

[76] There is no uniform definition of a “cruise” in the GLODAP data base. For example, WOCE section P6 in the South Pacific, which is treated here as a single cruise, is often divided into three cruises with subdesignations of E, C, and W for east, central, and west, respectively. Alternately, one might refer to WOCE section P17 along 135°W, which is here designated as portions of several cruises including P17N, P17C, P16S17S, P16A17A, and P17E19S. Since there is no optimal scheme for all situations, we have retained the names adopted over the years as the data set

developed. Sufficient information to identify the cruises is given in the files that are available at the website with the data. Given the confusion that exists in various compilations, the user is strongly encouraged to refer to the EXPOCODE for final identification, cross indexing, etc. EXPOCODE reference is particularly important in the Atlantic.

A2. Sources

[77] Most of the data included in the GLODAP data sets came from six sources (1) the WOCE Hydrographic Program Office (WHP) (<http://whpo.ucsd.edu/>), the primary source for hydrographic data, nutrients, oxygen, station information for WOCE cruises; (2) CDIAC (<http://cdiac.esd.ornl.gov/oceans/home.html>), the primary source for carbon measurements including DIC, TA, pH, and pCO₂; (3) the JGOFS data office (<http://usjgofs.whoi.edu/jg/dir/jgofs/>), for all information pertaining to JGOFS cruises (excluding EqPac spring and EqPac fall cruises); (4) the NOAA offices involved in OACES (<http://www.aoml.noaa.gov/ocd/oaces> and <http://www.pmel.noaa.gov/co2/co2-home.html>), which are now referred to as GCC (Global Carbon Cycle), primary source for hydrographic data, nutrients, oxygen, station information for OACES cruises; (5) the National Ocean Sciences Accelerator Mass Spectrometer (NOSAMS) office for all small volume radiocarbon data; and (6) data originators and/or chief scientists, for isotopic data and any preliminary versions of any data.

[78] The data sets developed simultaneously with data collection and have been updated as data processing progressed. WOCE and OACES cruise files were often initiated with preliminary (shipboard) versions of the hydrographic data. Carbon parameters and tracer data were received directly from the investigator who made the measurements and were merged with existing hydrography. When quality-controlled hydrography or carbon data became available, these parameters in the database were updated. This procedure allowed research to begin at a much earlier date; however, it allows the possibility, or more likely probability, that the GLODAP data sets do not include the latest version of all corrections/updates. In spite of this potential problem, we believe that the adopted procedure was both prudent and beneficial. Benefit derived from the fact that different people using different procedures and software were forced to critically evaluate the data. This duplicated effort resulted in many data errors such as data entry, parameter units, and data identification being corrected which otherwise would have been overlooked, or at least not found so quickly (A. Kozyr of CDIAC deserves special recognition along these lines for his efforts in helping WHP keep its version of the carbon results updated). We have maintained detailed records of the various updates, but have not attempted to document them here. Records for changes to the official WHP data files can be found at the above listed internet WOCE site.

[79] Unlike the WOCE and OACES data files, the JOGFS cruise data were downloaded (January 2002) from the website after the data were declared final. No adjustments or corrections of any type were made to the JOGFS files other than to assign flag values of “2” (good) to all the existing measurements. Not all JGOFS cruise data are included in this

compilation. Relative to the other projects, JGOFS sampled a large number of stations in a few relatively small areas. JGOFS program design also required sampling a region during different seasons. Rather than attempt to deal with the weighting biases that could result from including all the data, we have selected a subset of the JGOFS cruises. Those cruises that contained the most information (parameters) of interest to this project were selected, as were those that filled data gaps left by the combined WOCE + OACES cruises.

A3. Organization

[80] The zero-order data organization is by ocean, Atlantic, Indian, and Pacific. The Southern Ocean is segregated into three components, with division occurring south of Patagonia (~70°W), Capetown, South Africa (~20°E), and Tasmania (~120°E). The exact boundary definition is not critical. In order to allow watermass investigation in the vicinity of the arbitrary Southern Ocean boundaries and to reduce edge effects during mapping, data from some cruises are included in more than one ocean data set. For example, the Atlantic data set, as well as the Indian, includes a copy of the data from the WOCE I6S section. These cross listings are indicated in the cruise files, which are available at the CDIAC website along with the data files. If one wanted to create a global data set by merging the three oceans, then these replicate listings should be eliminated.

[81] Within each ocean the cruise files are sorted by cruise, then station occupation date, and then pressure. The cruise sorting is WOCE + OACES, followed by JGOFS (if any), and ending with historical. Within these categories the exact cruise sequence is arbitrary. Within each ocean data set, each cruise has been assigned a sequential integer identification number (see the second column, “No.” in the cruise files that are available at the CDIAC website with the data files) rather than including the actual cruise name or EXPOCODE. This substitution allows the data files to be purely numeric rather than alphanumeric. This substitution requires that one have a lookup table to identify a specific cruise, but greatly simplifies any other coding required to work with these rather large data sets. To provide compatibility with some existing software, the original station numbers have been altered systematically to guarantee that each station number in each data set is unique. In almost all instances the new station number was derived by equation (A1). In these instances the original station number is then simply derived by equation (A2). Within a cruise the station ordering was not required to be ascending, but usually is. In a few instances, some of the original station “numbers” were alphanumeric. Whenever possible, the alphabetic portion of the number was simply dropped. In the few instances where dropping the alphabetic portion resulted in a duplicate station number for that cruise or where the original data contained multiple occupations of the same location at different times and that location was assigned the same station number in each instance, new station numbers were fabricated.

$$N = 1000(C - 1) + O \quad (\text{A1})$$

$$O = \text{Modulo}(N, 1000), \quad (\text{A2})$$

Table A1. WOCE Flag Summary

Flag	Meaning
0	calculated which could have been measured
1	sample collected
2	good value
3	questionable value
4	bad value
5	no reported result
6	replicate result
7	manual chromatographic peak integration
8	irregular digital peak integration
9	no sample collected

where N is the new station number, C is the cruise number, and O is the original station number.

A4. WOCE QC Flag Values

[82] All measured parameters on WOCE cruises were assigned quality control (QC) flags using the values summarized in Table A1. OACES cruises were similarly flagged, JGOFS and all historical cruises did not have assigned QC flags. In these cases all existing measured values were flagged “good.” Historical cruise data was subjected to minor QC checking, but the procedure was generally much less careful than used for WOCE cruises. All of the carbon data were independently QC’ed by Princeton and CDIAC then any differences were mutually resolved.

[83] The QC flag value “0” did not exist in the original WOCE definitions. It was suggested by GLODAP and subsequently adopted by WHP. Our original definition and the way it is used in these data sets is: a flag value of “0” indicates a “good” value that could have been measured, but was somehow calculated. An exception to this rule is when TA was calculated from measured DIC and either pH or pCO₂ using thermodynamic relationships. These TA values were flagged as if they had been measured on the assumption that no additional significant error was incurred in the calculation. In practice, the flag values “1,” “7,” and “8” were not used very often, and “9” was generally used in stead of “5.” During data checking, flag assignment of “3” or “4” was subjective and depended upon the overall quality of the entire set of values for each parameter. Originally, “4” was intended to indicate that something was known to have caused a bad result as documented by various lab records. This proved far too cumbersome, and the choice between “3” or “4” evolved into a data expert’s opinion on whether the result was “questionable or thought bad” or “almost certainly bad.” Calculated values that could not be measured, such as anthropogenic CO₂, were flagged either “2,” “3,” “4,” or “9” in the master files. During the cruise merge procedure the QC flags listed in Table A1 were simplified to the subset values “0,” “2,” and “9” (see main text).

A5. Calculated Values

[84] Whenever data from a new cruise were obtained, routinely calculated values including potential temperature, potential density, and AOU were discarded then recalculated. This guaranteed uniformity. In a very few instances

(historic cruises) the files did not contain measured temperature values and the original potential temperature values had to be accepted. Potential temperature calculations used the functions of *Fofonoff* [1977] and the adiabatic lapse rate from *Bryden* [1973]. Potential density calculations used the *U.N. Educational, Scientific, and Cultural Organization* [1981] function and AOU used the solubility the function of *Garcia and Gordon* [1992].

[85] With each new data set, we tried to verify that the stated units were correct. This was a significant problem only with nutrient values and persisted throughout the WOCE era. Historically, most physical oceanographers preferred nutrient concentrations in micromole/liter while chemical oceanographers, since GEOSECS, have generally used micromole/kilogram. With many older data sets, the difference (~2%) is negligible relative to the measurement precision, but this is not the case with modern measurements (the WOCE criterion for nutrient precision is 2%). In some instances, the only way to resolve the question was direct communication with the person who made the measurements and could check the original shipboard data. With oxygen data the same problem exists between units of milliliters liter⁻¹ or micromoles kilogram⁻¹; however, differentiation in this case was always trivial. A more subtle problem exists with nitrate measurements. Some data sets include nitrate + nitrite in a field labeled “nitrate,” some list both separately, and others have a field defined as “NO₃ + NO₂”. Wherever possible, nitrate and nitrite have been separated. When separation was impossible, the sum is listed in the GLODAP data as “nitrate” and the nitrite values are listed as missing (−9). We do not include that information here, but it is frequently available at the various data centers. Nitrite values included in the GLODAP data files received minimal attention.

[86] On most WOCE cruises the date, time, location, and bottom depth were recorded at the beginning and end of each cast as well as when the cast reached the maximum lowering depth. The GLODAP files include data recorded when the cast was at its deepest. The “bottom depth” values recorded in the data files are only approximate and derived from numerous sources. When available, these values were taken from original data files; however, many values have been altered to be slightly deeper than the deepest sample depth, and some were taken from global topographies. The values are generally sufficiently accurate to generate a bottom mask for sections or maps, but not much more. Any attempt to reference samples to “distance off the bottom” should be done with extreme caution and expecting significant errors in a few instances.

[87] Radiocarbon separation used the functions given by *Rubin and Key* [2002] where alkalinity data existed. In the absence of alkalinity data, the *Broecker et al.* [1995] silicate method was used so long as the sampling latitude was equatorward of 45° latitude. Silicate-based estimates were adjusted to match the potential alkalinity estimates using the relationship from *Rubin and Key* [2002, equation (4), Figure 16]. Bomb ¹⁴C is included in the data files in two columns (‰ and 10⁹ atom meter⁻³). The listing in permil is primarily for display purposes and was calculated with equation (A3). *Broecker et al.* [1995] referred to this

quantity as $\Delta\Delta^{14}\text{C}(\text{‰})$. The total absence of bomb ^{14}C as calculated by equation (A3) is 0‰ rather than $\sim -1000\text{‰}$.

$$\Delta^{14}C_{\text{Measured}}(\text{‰}) = \Delta^{14}C_{\text{Natural}}(\text{‰}) + {}^{14}C_{\text{Bomb}}(\text{‰}). \quad (\text{A3})$$

[88] To get bomb radiocarbon in mass units, convert the measured $\Delta^{14}\text{C}$ and natural $\Delta^{14}\text{C}$ to mass units then subtract. These conversions are included in the data files where the calculation was performed on a per sample basis using equations (A4)–(A6).

$$\Delta^{14}\text{C} = \delta^{14}\text{C} - 2(\delta^{13}\text{C} + 25) \left(1 + \frac{\delta^{14}\text{C}}{1000}\right) \quad (\text{A4})$$

$$\delta^{14}\text{C} = \left(\frac{{}^{14}\text{C}/{}^{12}\text{C}}{0.95\text{STD}}\right) 1000. \quad (\text{A5})$$

Let $x = 2(\delta^{13}\text{C} + 25)$; then

$${}^{14}\text{C} = \left(\frac{\Delta^{14}\text{C} + x}{1000 - x} + 1\right) \bullet 0.95\text{STD} \text{ }^{12}\text{C}\rho k, \quad (\text{A6})$$

where ${}^{12}\text{C}$ is DIC ($\mu\text{mole kg}^{-1}$), STD is the oxalic acid standard with a ratio of 1.176×10^{-12} , ρ is density (kg liter^{-1}), and k is the constant necessary to convert units, in this case, $\mu\text{mole liter}^{-1}$ to 10^9 atoms meter³, so $k = 6.02 \times 10^{11}$. Wherever possible, measured values were used for the conversion; however, in the case of missing or questionable data, 1.028 was used for density, and 0.8‰ (0–1000 meter depth) or 0.3‰ (depth >1000 meter) for $\delta^{13}\text{C}$, and DIC was approximated using equation (A7), which was derived from a least squares fit to the global WOCE data (multiple $R^2 = 0.946$, residual standard error = 23.3). These estimated DIC values were only used in the radiocarbon calculations and were not saved in the data tables. The $\delta^{13}\text{C}$ values are global means based on WOCE measurements. Any bomb radiocarbon estimate that had a calculated value less than zero (‰) was reset to zero in the data files.

$$\text{DIC} \approx 723.3013 + 36.6594\text{Sa} + 0.4412\text{Si} + 7.0201\text{Ni}, \quad (\text{A7})$$

where Sa is salinity, Si is silicate, and Ni is nitrate.

[89] CFC partial pressures and ages were based on the solubilities of Warner and Weiss [1985] and the atmospheric time history from Walker et al. [2000]. The CFC age is estimated by matching the measured CFC partial pressure in a water sample to an atmospheric CFC partial pressure history. The time difference between that match point and sample collection date is the CFC age. The calculation assumes that surface waters equilibrate with the atmosphere by gas exchange prior to sinking/subduction. For additional information on this calculation including the assumptions, see Doney and Bullister [1992] and Warner et al. [1996]. Important discrepancies between CFC ages and “true ages” under certain circumstances are discussed by Matear and McNeil [2003], Matear et al. [2003], Hall et al. [2002], and references therein. Errors in the CFC ages

are incorporated into the anthropogenic CO_2 estimates due to the methodology.

[90] Calculated values were assigned a flag value equal to the worst of the flags associated with the input parameters. For example, potential alkalinity is calculated with equation (A8).

$$\text{PA} = (\text{A} + \text{Ni}) \times 35 \text{ Sa}, \quad (\text{A8})$$

where PA is potential alkalinity, A is alkalinity, Ni is nitrate, and Sa is salinity. If the alkalinity flag was “6” (good replicate), the nitrate flag was “2” (good), and the salinity flag was “3” (questionable), then the potential alkalinity flag was set to “3.”

A6. Calibration

[91] Calibration factors are summarized in tables with the other metadata files at CDIAC. Atlantic factors for salinity, oxygen, and nutrients were taken from Gouretski and Jancke [2001]. The Indian/Pacific factors were from Johnson et al. [2001] and subsequent unpublished work on the WOCE Indian Ocean nutrients by C. Mordy and L. Gordon (personal communication, 2003). Each of these studies used an objective procedure to minimize cruise crossover differences on a basin scale. Note that the Gouretski and Jancke [2001] correction factors are additive and the latter (except for salinity) are multiplicative. These efforts were based on the assumption of steady state for deep waters.

[92] The calibration factors applied to the carbon data (DIC and TA) were derived more subjectively using evidence from several different comparison methods. Johnson et al. [1998] and Millero et al. [1998a] examined the quality of the WOCE Indian Ocean DIC and TA results, respectively. Sabine et al. [1999] added comparison for WOCE cruises S4I and I6, and for the historical INDIGO and GEOSECS expeditions. In short, there were no adjustments necessary for any of the WOCE Indian Ocean carbon measurements. The WOCE Pacific carbon adjustments were taken from Sabine et al. [2002a] and the Atlantic from Wanninkhof et al. [2003]. In all cases, the carbon adjustments are additive. In a few instances, the carbon calibration efforts concluded that certain cruise data were either too noisy or too far out of calibration for adjustment to be advisable. In these cases, the investigators recommended that the data not be used, and that suggestion was followed in this and all related GLODAP publications.

A7. Vertical Interpolation

[93] Once all the data for a cruise was assembled and calibrated, missing values for salinity, oxygen, and nutrients were interpolated when practical. “What is practical” is defined below. First, the existing data (parameters flagged “good” or “replicate” and accompanying pressures) were fit with a smooth curve (quasi-Hermitian-piecewise polynomial) that was subsequently evaluated at all pressures that had missing values. The interpolated values were then subjected to a “nearest neighbors” rejection criterion that varied with pressure as summarized in Table A2. For example, if a bottle at 400 db was missing salinity and the nearest bottles above and below with acceptable salinity

Table A2. Interpolation Rejection Criteria

Pressure Range, Decibars	Maximum Neighbor Separation
0–200.99	100
201–750.99	200
751–1500.99	250
1501–12000	500

values (good or replicate) were at 300 and 550 dB, then the interpolated value would be rejected because the nearest neighbor separation distance is 250 (550 – 300) and the maximum allowable separation for that pressure range is 200 dB. All interpolated values were assigned a QC flag value of “0” (see Table A1).

Appendix B

[94] Vertical data interpolation onto the mapping surface depths used the same algorithm described in Appendix A. For the $\Delta^{14}\text{C}$ and bomb ^{14}C maps, the allowable maximum data separation distances (column 2 of Table A2) were increased to 300, 500, 500, and 1000 meters due to reduced data density. During this interpolation, only those input data flagged “0” or “2” (approximated or good; recall that replicate flags “6” had already been translated to “2”) were considered. The specific map surfaces are the same 33 as used by *Conkright et al.* [2002].

[95] After vertical interpolation of the data onto the depth surfaces, the data were horizontally gridded using the objective analysis procedure of *Sarmiento et al.* [1982]. The grid resolution was 1° latitude by 1° longitude with grid centers at 0.5° . Gridding was restricted to the convex hull occupied by station data (approximately) and was manually defined. Adjacent seas (Gulf of Mexico, Caribbean Sea, Mediterranean Sea, Indonesian Seas, etc.), the far North

Atlantic (north of the southern edge of Iceland), and the Arctic Ocean were excluded because the GLODAP compilation has either no data or extremely limited data for these regions. The actual mapping procedure involves inversion of a large matrix and has significant computer memory requirements because the calculation is done in double precision. This computation is one of the primary reasons that each ocean was mapped independently rather than mapping the entire globe at once. An added benefit of mapping the oceans independently is that it eliminates ocean to ocean data influence (“crosstalk”), especially across narrow bands of land. In the deep ocean, crosstalk through ocean ridges also presents problems. The situation is especially acute in the Atlantic where deep western basin properties differ significantly from those in the eastern basin. For the deep Atlantic only, the eastern and western basins were mapped separately to minimize crosstalk. It would have been preferable to do the same in the deep Indian Ocean, but the data density is insufficient.

[96] The limited data density required that long correlation length scales be used for the mapping procedure. This in turn results in very significant smoothing of the mapped fields. This problem has been noted in previous climatologies, but is even worse with the GLODAP maps. The procedure does not require that measured values in specific grid cells be reproduced in the gridded result. One consequence of the smoothing is that property extrema are almost always reduced in magnitude. In certain circumstances, the mapping procedure can exhibit “ringing.” When it occurs, it is in areas relatively far removed from measurements or near the map boundaries, that is, where the procedure extrapolates rather than interpolates.

[97] The objective analysis procedure returns an error for each grid cell. Because of the underlying assumptions of the calculation, these errors are only approximate and probably

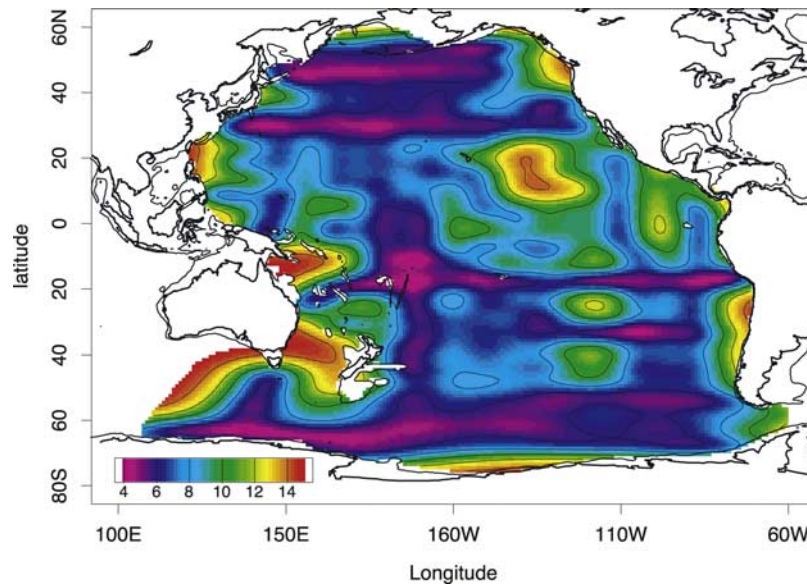


Figure B1. Estimated error field for the Pacific Ocean TA distribution at 1200 m (see Figure 2, left center, for the corresponding property map). Note that the size of the error is strongly correlated with distance from data. These mapping error estimates assume no measurement or other error types.

underestimate the real uncertainty in most cases. In spite of these problems, the error fields should not be ignored. For any given map, the magnitude of a grid cell error has meaning relative to the other cell errors. Even a cursory investigation of any of the error fields easily demonstrates the error increases as the distance from data increases. Visual inspection of an error field is also sufficient to demonstrate the high degree of correlation among the individual error estimates. Routine error propagation calculations require independent errors; therefore, such calculation should not be made with the mapping error estimates. An example of an error map is given in Figure B1, which shows the TA error at 1200 m for the Pacific Ocean (corresponding to the left center plot of Figure 3). The estimated errors range from 4 to 15 $\mu\text{mole kg}^{-1}$. This is small compared to the mean TA concentration on this surface (2357 $\mu\text{mole kg}^{-1}$), but rather significant when compared to the total TA concentration range on this surface (Pacific only), which is 91 $\mu\text{mole kg}^{-1}$. The large errors south of Australia are an example of the ringing discussed above. The error fields are posted along with the field estimates at CDIAC.

[98] **Acknowledgments.** Data for this effort were contributed by hundreds of scientists and technicians, including many international colleagues; however, the authors bear responsibility for errors of omission and/or commission. A complete listing of the funded grants that supported this research would require yet another Appendix. Alternately, we gratefully recognize the generous support received from the National Science Foundation, the National Oceanic and Atmospheric Administration, the Department of Energy, the National Aeronautics and Space Administration, and the Office of Naval Research by the various authors and other participants over the past 15 years. Special thanks is given to Doug Wallace, who was the U.S. CO₂ Science Team leader for much of this project, and to his predecessor John Downing, who originally organized the science team. Downing's efforts to acquire SOMMAs for the various research groups and his support for the CRM program were also critical to the success of this project. Recognition is also given to other science team members David Chipman, Andrew Dickson, Catherine Goyet, Peter Guenther, Ken Johnson, Charles Keeling, Taro Takahashi, and Chris Winn. The cruise chief scientists and principal investigators for the carbon, nutrient, dissolved oxygen, and CFC programs are listed in the cruise tables available online at CDIAC. The high quality of the data set is due in large part to the many dedicated analysts who participated on these cruises. Special recognition is deserved for the shipboard teams from Scripps (Ocean Data Facility) and WHOI and for the support personnel at both the WOCE and JGOFS hydrographic data offices. Special mention of Lou Gordon is deserved for his extremely valuable insight and guidance regarding all nutrient matters, not to mention the many measurements his group made. Thoughtful input from Niki Gruber at various stages of the anthropogenic CO₂ calculations was extremely helpful. Rick Slater provided the masks and ferret code used to produce the mean profile figures. Anna Vilerio was instrumental in final document preparation. This publication is NOAA/PMEL contribution 2665 and JISAO contribution 1050. Recent support for R. M. Key was primarily from NOAA NA96GP0200 and NSF OCE9819144, OCE 9986310, and OCE0136617.

References

- Brewer, P. G., and J. C. Goldman (1976), Alkalinity changes generated by phytoplankton growth, *Limnol. Oceanogr.*, *21*, 108–117.
- Broecker, W. S. (2003), The oceanic CaCO₃ cycle, in *Treatise on Geochemistry*, edited by H. D. Holland and K. K. Turekian, vol. 6, pp. 1–21, Pergamon, New York.
- Broecker, W. S., S. Sutherland, W. Smethie, T.-H. Peng, and G. Östlund (1995), Oceanic radiocarbon: Separation of the natural and bomb components, *Global Biogeochem. Cycles*, *9*(2), 263–288.
- Bryden, H. L. (1973), New polynomials for thermal expansion, adiabatic temperature gradient and potential temperature of sea water, *Deep Sea Res.*, *20*, 401–408.
- Chung, S., K. Lee, R. A. Feely, C. L. Sabine, F. J. Millero, R. M. Key, and R. Wanninkhof (2003), Calcium carbonate budget in the Atlantic Ocean based on water-column inorganic carbon chemistry, *Global Biogeochem. Cycles*, *17*(4), 1093, doi:10.1029/2002GB002001.
- Chung, S.-N., G.-H. Park, K. Lee, R. M. Key, F. J. Millero, R. A. Feely, C. L. Sabine, and P. G. Falkowski (2004), Postindustrial enhancement of aragonite undersaturation in the upper tropical and subtropical Atlantic Ocean: The role of fossil fuel CO₂, *Limnol. Oceanol.*, *49*, 15–321.
- Conkright, M. E., et al. (2002), *World Ocean Database 2001*, vol. 1, *Introduction*, edited by S. Levitus, NOAA Atlas NESDIS 42, 167 pp., Natl. Oceanic and Atmos. Admin., Silver Spring, Md.
- Craig, H. (1972), The GEOSECS Program: 1970–1971, *Earth Planet. Sci. Lett.*, *16*, 47–49.
- Craig, H. (1974), The GEOSECS Program: 1972–1973, *Earth Planet. Sci. Lett.*, *23*, 63–64.
- Craig, H., and K. K. Turekian (1976), The GEOSECS program: 1973–1976, *Earth Planet. Sci. Lett.*, *32*, 217–219.
- Craig, H., and K. K. Turekian (1980), The GEOSECS program: 1976–1979, *Earth Planet. Sci. Lett.*, *49*, 263–265.
- Department of Energy (1994), *Handbook of Methods for the Analysis of the Various Parameters of the Carbon Dioxide System in Sea Water, Version 2*, edited by A. G. Dickson and C. Goyet, ORNL/CDIAC-74, Carbon Dioxide Inf. and Anal. Cent., Oak Ridge, Natl. Lab., Oak Ridge, Tenn.
- Dickson, A. G. (2001), Reference materials for oceanic CO₂ measurements, *Oceanography*, *14*(4), 21–22.
- Dickson, A. G., and F. J. Millero (1987), A comparison of the equilibrium constants for the dissociation of carbonic acid in seawater media, *Deep Sea Res.*, *34*, 1733–1743.
- Dickson, A., J. D. Afghan, and G. C. Anderson (2003), Reference materials for oceanic CO₂ analysis: A method for the certification of total alkalinity, *Mar. Chem.*, *80*, 185–197.
- Doney, S. C., and J. L. Bullister (1992), A chlorofluorocarbon section in the eastern North Atlantic, *Deep Sea Res.*, *39*, 1857–1883.
- Dutay, J.-C., et al. (2002), Evaluation of ocean model ventilation with CFC-11: Comparison of 13 global ocean models, *Ocean Modell.*, *4*, 89–120.
- Feely, R. A., C. L. Sabine, T. Takahashi, and R. Wanninkhof (2001), Uptake and storage of carbon dioxide in the oceans: The global CO₂ survey, *Oceanography*, *14*(4), 18–32.
- Feely, R. A., et al. (2002), In-situ calcium carbonate dissolution in the Pacific Ocean, *Global Biogeochem. Cycles*, *16*(4), 1144, doi:10.1029/2002GB001866.
- Feely, R. A., C. L. Sabine, K. Lee, W. Berelson, J. Kleypas, V. J. Fabry, and F. J. Millero (2004), The impact of anthropogenic CO₂ on the CaCO₃ system in the oceans, *Science*, *305*, 362–366.
- Fiadiero, M. E. (1982), Three-dimensional modeling of tracers in the deep Pacific Ocean: Radiocarbon and the circulation, *J. Mar. Res.*, *40*, 537–550.
- Fofonoff, N. P. (1977), Computation of potential temperature of seawater for an arbitrary reference pressure, *Deep Sea Res.*, *24*, 489–491.
- Gandin, L. S. (1963), *Objective Analysis of Meteorological Fields*, 286 pp., Hydrometeoizdat, St. Petersburg, Russia.
- Garcia, H. E., and L. I. Gordon (1992), Oxygen solubility in seawater: Better fitting equations, *Limnol. Oceanogr.*, *37*, 1307–1312.
- Gouretski, V. V., and K. Jancke (2001), Systematic errors as the cause for an apparent deep water property variability: Global analysis of the WOCE and historical hydrographic data, *Prog. Oceanogr.*, *48*, 337–402.
- Goyet, C., and S. D. Hacker (1992), Procedure for calibration of a coulometric system used for total inorganic carbon measurements of seawater, *Mar. Chem.*, *38*, 37–51.
- Goyet, C., R. Healy, and J. Ryan (2000), Global distribution of total inorganic carbon and total alkalinity below the deepest winter mixed layer depths, ORNL/CDIAC-127, 28 pp., Carbon Dioxide Inf. Anal. Cent., Oak Ridge Natl. Lab., Oak Ridge, Tenn.
- Gruber, N. (1998), Anthropogenic CO₂ in the Atlantic Ocean, *Global Biogeochem. Cycles*, *12*(1), 165–191.
- Gruber, N., J. L. Sarmiento, and T. F. Stocker (1996), An improved method for detecting anthropogenic CO₂ in the oceans, *Global Biogeochem. Cycles*, *10*(4), 809–837.
- Hall, T. M., T. W. N. Haine, and D. W. Waugh (2002), Inferring the concentration of anthropogenic carbon in the ocean from tracers, *Global Biogeochem. Cycles*, *16*(4), 1131, doi:10.1029/2001GB001835.
- Jenkins, W. J. (1998), Studying subtropical thermocline ventilation and circulation using tritium and ³He, *J. Geophys. Res.*, *103*, 15,817–15,832.
- Johnson, G. C., P. E. Robbins, and G. E. Hufford (2001), Systematic adjustments of hydrographic sections for internal consistency, *J. Atmos. Oceanic Technol.*, *18*, 1234–1244.

- Johnson, K. M., K. D. Willis, D. B. Butler, W. K. Johnson, and C. S. Wong (1993), Coulometric total carbon dioxide analysis for marine studies: Maximizing the performance of an automated gas extraction system and coulometric detector, *Mar. Chem.*, *44*, 167–187.
- Johnson, K. M., et al. (1998), Coulometric total carbon dioxide analysis for marine studies: Assessment of the quality of total inorganic carbon measurements made during the US Indian Ocean CO₂ survey 1994–1996, *Mar. Chem.*, *63*, 21–37.
- Joyce, T., and C. Corry (Eds.) (1994), Requirements for WOCE Hydrographic Programme Data Reporting, *WHPO Pub. 90-1 Rev. 2*, 145 pp., WOCE Hydrogr. Programme Off., La Jolla, Calif.
- Kawasi, M., and J. L. Sarmiento (1985), Nutrients in the Atlantic thermocline, *J. Geophys. Res.*, *90*, 8961–8976.
- Kawasi, M., and J. L. Sarmiento (1986), Circulation and nutrients in mid-depth Atlantic waters, *J. Geophys. Res.*, *91*, 9749–9770.
- Key, R. M. (1996), WOCE Pacific Ocean radiocarbon program, *Radiocarbon*, *38*(3), 415–423.
- Key, R. M. (1997), Changes in the Pacific Ocean distribution of radiocarbon since GEOSECS, 1997, *U.S. WOCE Implement. Rep. 9*, U.S. World Ocean Circ. Exp. Off., College Station, Texas.
- Key, R. M. (2001), Ocean process tracers: Radiocarbon, in *Encyclopedia of Ocean Sciences*, edited by J. Steele, S. Thorpe, and K. Turekian, pp. 2338–2353, Academic, San Diego, Calif.
- Key, R. M., P. D. Quay, G. A. Jones, A. P. McNichol, K. F. Von Reden, and R. J. Schneider (1996), WOCE AMS Radiocarbon I: Pacific Ocean results; P6, P16 & P17, *Radiocarbon*, *38*(3), 425–518.
- Key, R. M., P. D. Quay, P. Schlosser, M. Stuiver, H. G. Östlund, J. Hayes, A. P. McNichol, K. F. Von Reden, and R. J. Schneider (2002), WOCE Radiocarbon IV: Pacific Ocean results; P10, P13N, P14C, P18, P19 & S4P, *Radiocarbon*, *44*(1), 239–392.
- Kroopnick, P. M. (1985), The distribution of ¹³C of ΣCO₂ in the world oceans, *Deep Sea Res.*, *32*, 57–84.
- Lee, K., F. J. Millero, and D. M. Campbell (1996), The reliability of the thermodynamic constants for the dissociation of carbonic acid in seawater, *Mar. Chem.*, *55*, 233–245.
- Lee, K., et al. (2003), An updated anthropogenic CO₂ inventory in the Atlantic Ocean, *Global Biogeochem. Cycles*, *17*(4), 1116, doi:10.1029/2003GB002067.
- LeTraon, P. Y. (1990), A method for optimal analysis of fields with spatially variable mean, *J. Geophys. Res.*, *95*, 13,543–13,547.
- Levitus, S., and T. P. Boyer (1994a), *World Ocean Atlas*, vol. 4, *Temperature*, NOAA Atlas NESDIS 4, Natl. Oceanic and Atmos. Admin., Silver Spring, Md.
- Levitus, S., and T. P. Boyer (1994b), *World Ocean Atlas*, vol. 2, *Oxygen*, NOAA Atlas NESDIS 2, Natl. Oceanic and Atmos. Admin., Silver Spring, Md.
- Levitus, S., R. Burgett, and T. P. Boyer (1994), *World Ocean Atlas*, vol. 3, *Salinity*, NOAA Atlas NESDIS 3, Natl. Oceanic and Atmos. Admin., Silver Spring, Md.
- Lewis, E., and D. W. R. Wallace (1998), Program developed for CO₂ system calculations, *ORNL/CDIAC-105*, 21 pp., Carbon Dioxide Inf. Anal. Cent., Oak Ridge Natl. Lab., Oak Ridge, Tenn.
- Matear, R. J., and B. J. McNeil (2003), Decadal accumulation of anthropogenic CO₂ in the Southern Ocean: A comparison of CFC-age derived estimates to multiple-linear regression estimates, *Global Biogeochem. Cycles*, *17*(4), 1113, doi:10.1029/2003GB002089.
- Matear, R. J., C. S. Wong, and L. Xie (2003), Can CFCs be used to determine anthropogenic CO₂?, *Global Biogeochem. Cycles*, *17*(1), 1013, doi:10.1029/2001GB001415.
- Matsumoto, K., and R. M. Key (2004), Natural radiocarbon distribution in the deep ocean, in *Global Environmental Change in the Ocean and on Land*, edited by M. Shiyomi et al., pp. 45–58, TERRAPUB, Tokyo.
- Matsumoto, K., et al. (2004), Evaluation of ocean carbon cycle models with data-based metrics, *Geophys. Res. Lett.*, *31*, L07303, doi:10.1029/2003GL018970.
- McDowell, S. E., and H. T. Rossby (1978), Mediterranean water: An intense mesoscale eddy off the Bahamas, *Science*, *202*, 1085–1087.
- McElligott, S., R. H. Byrne, K. Lee, R. Wanninkhof, F. J. Millero, and R. A. Feely (1998), Discrete water column measurements of CO₂ fugacity and pH_T in seawater: A comparison of direct measurements and thermodynamic calculations, *Mar. Chem.*, *60*, 63–73.
- McNeil, B. I., R. J. Matear, R. M. Key, J. L. Bullister, and J. L. Sarmiento (2003), Anthropogenic CO₂ uptake by the ocean based on the global chlorofluorocarbon dataset, *Science*, *299*, 235–239.
- Mehrbach, C., C. H. Culbertson, J. E. Hawley, and R. M. Pytkowicz (1973), Measurements of the apparent dissociation constants of carbonic acid in seawater at atmospheric pressure, *Limnol. Oceanogr.*, *18*, 897–907.
- Millero, F. J., et al. (1998a), Assessment of the quality of the shipboard measurements of total alkalinity on the WOCE Hydrographic Program CO₂ survey cruises 1994–1996, *Mar. Chem.*, *63*, 9–20.
- Millero, F. J., K. Lee, and M. P. Roche (1998b), Distribution of alkalinity in the surface waters of the major oceans, *Mar. Chem.*, *60*, 111–130.
- Millero, F. J., D. Pierrot, K. Lee, R. Wanninkhof, R. Feely, C. L. Sabine, R. M. Key, and T. Takahashi (2002), Dissociation constants for carbonic acid determined from field measurements, *Deep Sea Res., Part I*, *49*, 1705–1723.
- Mojica Prieto, F. J., and F. J. Millero (2002), The values of pK₁ + pK₂ for the dissociation of carbonic acid in seawater, *Geochim. Cosmochim. Acta*, *66*(14), 2529–2540.
- Murnane, R. J., J. L. Sarmiento, and C. LeQuere (1999), Spatial distribution of air-sea CO₂ fluxes and the interhemispheric transport of carbon by the oceans, *Global Biogeochem. Cycles*, *13*(2), 287–305.
- Orr, J. C., et al. (2001), Estimates of anthropogenic carbon uptake from four three-dimensional global ocean models, *Global Biogeochem. Cycles*, *15*(1), 43–60.
- Östlund, H. G., and C. G. H. Rooth (1990), The North Atlantic tritium and radiocarbon transients 1972–1983, *J. Geophys. Res.*, *95*, 20,147–20,166.
- Robinson, C., and P. J. L. B. Williams (1991), Development and assessment of an analytical system for the accurate and continual measurement of total dissolved inorganic carbon, *Mar. Chem.*, *34*, 157–175.
- Roussinov, V., R. G. Williams, M. J. Follows, and R. M. Key (2004), Role of bottom water transport and diapycnic mixing in determining the radiocarbon distribution in the Pacific, *J. Geophys. Res.*, *109*, C06015, doi:10.1029/2003JC002188.
- Rubin, S., and R. M. Key (2002), Separating natural and bomb-produced radiocarbon in the ocean: The potential alkalinity method, *Global Biogeochem. Cycles*, *16*(4), 1105, doi:10.1029/2001GB001432.
- Sabine, C. L., F. T. Mackenzie, C. Winn, and D. M. Karl (1995), Geochemistry of carbon dioxide in seawater at the Hawaii time series station, ALOHA, *Global Biogeochem. Cycles*, *9*(4), 637–651.
- Sabine, C. L., R. M. Key, K. Johnson, F. J. Millero, J. Sarmiento, D. Wallace, and C. Winn (1999), Anthropogenic CO₂ inventory of the Indian Ocean, *Global Biogeochem. Cycles*, *13*(1), 179–198.
- Sabine, C. L., R. A. Feely, R. M. Key, J. L. Bullister, F. J. Millero, K. Lee, T.-H. Peng, B. Tilbrook, T. Ono, and C. S. Wong (2002a), Distribution of anthropogenic CO₂ in the Pacific Ocean, *Global Biogeochem. Cycles*, *16*(4), 1083, doi:10.1029/2001GB001639.
- Sabine, C. L., R. M. Key, R. A. Feely, and D. Greely (2002b), Inorganic carbon in the Indian Ocean: Distribution and dissolution processes, *Global Biogeochem. Cycles*, *16*(4), 1067, doi:10.1029/2002GB001869.
- Sabine, C. L., et al. (2004), The oceanic sink for anthropogenic CO₂, *Science*, *305*, 367–370.
- Sarmiento, J. L. (1983), A simulation of bomb tritium entry into the Atlantic Ocean, *J. Phys. Oceanogr.*, *13*(10), 1924–1939.
- Sarmiento, J. L., J. Willebrand, and S. Hellerman (1982), Objective analysis of tritium observations in the Atlantic Ocean during 1971–1974, *Tech. Rep. 1*, 19 pp., Ocean Tracer Lab., Princeton, N. J.
- Sarmiento, J. L., N. Gruber, M. A. Brzezinski, and J. P. Dunne (2004), High-latitude controls of thermocline nutrients and low latitude biological productivity, *Nature*, *427*, 56–60.
- Schlitzer, R. (1987), Renewal rates of east Atlantic deep water estimated by inversion of ¹⁴C data, *J. Geophys. Res.*, *92*, 2953–2969.
- Schlitzer, R. (2000), Electronic Atlas of WOCE Hydrographic and Tracer Data Now Available, *Eos Trans. AGU*, *81*, 45.
- Schlosser, P., J. L. Bullister, R. Fine, W. J. Jenkins, R. Key, J. Lupton, W. Roether, and W. M. Smethie Jr. (2001), Transformation and age of water masses, in *Ocean Circulation and Climate: Observing and Modelling the Global Ocean*, edited by G. Siedler, J. Church, and J. Gould, pp. 431–452, Academic, San Diego, Calif.
- Srinivasan, A., C. G. H. Rooth, Z. Top, and D. B. Olson (2000), Abyssal upwelling in the Indian Ocean: Radiocarbon diagnostics, *J. Mar. Res.*, *58*, 755–778.
- Stuiver, M., G. Östlund, R. M. Key, and P. J. Reimer (1996), Large volume WOCE radiocarbon sampling in the Pacific Ocean, *Radiocarbon*, *38*(3), 519–561.
- Toggweiler, J. R., and B. Samuels (1993), New radiocarbon constraints on the upwelling of abyssal water to the ocean's surface, in *The Global Carbon Cycle, NATO ASI Ser. I*, vol. 15, edited by M. Heimann, pp. 333–366, Springer-Verlag, New York.
- U.N. Educational, Scientific, and Cultural Organization (1981), Tenth report of the joint panel on oceanographic tables and standards, *UNESCO Tech. Pap. Mar. Sci.*, *36*, 13–21.
- Walker, S. J., R. F. Weiss, and P. K. Salameh (2000), Reconstructed histories of the annual mean atmospheric mole fractions for the halocarbons

- CFC-11, CFC-12 and carbon tetrachloride, *J. Geophys. Res.*, *105*, 14,285–14,296.
- Wanninkhof, R., E. Lewis, R. A. Feely, and F. J. Millero (1998), The optimal carbonate dissociation constants for determining surface water pCO₂ from alkalinity and total inorganic carbon, *Mar. Chem.*, *65*, 291–301.
- Wanninkhof, R., T.-H. Peng, B. Huss, C. L. Sabine, and K. Lee (2003), Comparison of inorganic carbon system parameters measured in the Atlantic Ocean from 1990 to 1998 and recommended adjustments, *ORNL/CDIAC-140*, 43 pp., Carbon Dioxide Inf. Anal. Cent., Oak Ridge Natl. Lab., Oak Ridge, Tenn.
- Warner, M. J., and R. F. Weiss (1985), Solubilities of chlorofluorocarbons 11 and 12 in water and seawater, *Deep Sea Res.*, *32*, 1485–1497.
- Warner, M. J., J. L. Bullister, D. P. Wisegarver, R. H. Gammon, and R. F. Weiss (1996), Basin-wide distributions of CFC-11 and CFC-12 in the North Pacific: 1985–1989, *J. Geophys. Res.*, *101*, 20,525–20,542.
- Wessel, P., and W. H. F. Smith (1991), Free software helps map and display data, *Eos Trans. AGU*, *72*, 579.
- Wessel, P., and W. H. F. Smith (1996), A global, self-consistent, hierarchical, high resolution shoreline database, *J. Geophys. Res.*, *101*, 8741–8743.
- Wessel, P., and W. H. F. Smith (1998), New version of the generic mapping tools released, *Eos Trans. AGU*, *79*, 579.
- Willey, D. A., R. A. Fine, R. E. Sonnerup, J. L. Bullister, W. M. Smethie Jr., and M. J. Warner (2004), Global oceanic chlorofluorocarbon inventory, *Geophys. Res. Lett.*, *31*, L01303, doi:10.1029/2003GL018816.
-
- J. L. Bullister, R. A. Feely, C. Mordy, and C. L. Sabine, Pacific Marine Environmental Laboratory, NOAA, Seattle, WA, USA.
- R. M. Key, Atmospheric and Oceanic Sciences, Princeton University, Princeton, NJ 08544, USA. (key@princeton.edu)
- A. Kozyr, Carbon Dioxide Information Analysis Center, Oak Ridge National Laboratory, Oak Ridge, TN, USA.
- K. Lee, School of Environmental Science and Engineering, Pohang University of Science and Technology, Pohang, Republic of Korea.
- F. J. Millero, Rosenstiel School of Marine and Atmospheric Sciences, University of Miami, Miami, FL, USA.
- T.-H. Peng and R. Wanninkhof, Atlantic Oceanographic and Meteorological Laboratory, NOAA, Miami, FL, USA.